Effects of Photodynamic Therapy with 5-Aminolevulinic Acid Hydrochloride on Primary Cultured Cells of Feline Mammary Tumors

ネコ乳腺腫瘍初代培養細胞に対する 5-アミノレブリン酸塩酸塩を用いた光線力学療法の効果

2024

Joint Graduate School of Veterinary Sciences, Tottori University

LIN, Siyao

CONTENTS

CONTENTS

SUMMARY

In Chapter 1, the authors described feline mammary tumors (FMT), photodynamic therapy (PDT), and three-dimensional (3D) culture. Most feline mammary tumors are malignant. Therefore, removing one or both sides of the mammary gland remains the mainstay treatment for eradicating mammary tumors. However, metastasis or recurrence is often observed post-surgery, with the postoperative prognosis being poor. Therefore, developing novel treatments to provide palliative care when tumors recur postoperatively is a necessity.

Photodynamic therapy using 5-aminolevulinic acid (5-ALA) is a tumor treatment that is low in toxicity and invasiveness. 5-ALA, protoporphyrin IX (PpIX) precursor, has been used in PDT because of its wide availability and safety. Photosensitizers (PS) preferentially accumulate in neoplastic tumor tissues based on their multiple factors. Three conditions are required to achieve PDT: PS, light, and oxygen. These three conditions are non-toxic when used alone. Still, the simultaneous action of the three can produce photochemical reactions, generating highly reactive and toxic ROS, including singlet oxygen, superoxide anion, hydroxyl radical, *etc*. PpIX has absorption peaks at 410, 510, 545, 580, and 630 nm, and 5-ALA-PDT usually uses light at a wavelength of 630 ± 5 nm for tumor therapy. PDT induces reactive oxygen species production by irradiating specific areas (areas of high PS concentration) with light, resulting in tumor cell apoptosis and necrosis, achieving the therapeutic goal, with minimal toxic side effects and low drug resistance. Clinically, PDT can be used in combination with surgery based on its mechanism of action. Despite decades of research, PDT has been poorly studied in FMT. Our aim was to assess the effectiveness of PDT using 5-ALA on FKR in primary cultured FMT and analyze the impact of tumor cell morphology on cell killing efficacy.

The most used tumor cell culture method in studies related to PDT is still the two-dimensionally (2D) model culture. 2D culture mainly has the advantages of simplicity of cell culture, low maintenance costs, and the ability to fulfill essential research testing functions. 2D culture mainly has the advantages of simplicity of cell culture, low maintenance costs, and the ability to fulfill essential research testing functions. However, under the conditions of 2D culture, tumor cells grown adherent to the flat surface on a flask or plate cannot mimic the natural structure of cellular tissues or tumors. Upon isolation from tissues and transfer to 2D conditions, the morphology of the cells is altered, and the pattern of cell division is changed. Altered cell morphology affects its function, the organization of intracellular structures, secretion, and cell signaling. In addition, alien to the *in-vivo* tumor microenvironment, due to the monolayer nature of 2D cultures, all cells in the culture receive equal amounts of oxygen, nutrients, and drugs. Oxygen concentration and the uptake of externally given photosensitizer by tumor cells are key factors affecting the therapeutic efficacy of 5-ALA-PDT, leading to the need for more suitable tumor cell culture models to enhance the accuracy of *in vitro* studies. *In vitro* studies, 2D cultures lack the ability to recapitulate the complexity of the tumor microenvironment, whereas 3D cultures models have overcome these limitations and are increasingly being applied in drug screening and oncology research. In Chapter 2, the author evaluated the cytotoxic effect of 5-ALA-PDT on FMT cells and influence of cell culture morphology differences on cell killing efficacy. Therefore, the author conducted a series of studies using 5-ALA-PDT on 2D cultured FKR-A and 3D cultured FKR-S FMT cells. FKR-A and FKR-S are homologous tumor cells, with the FKR cells extracted from the same FMT tissue.

In the *in vitro* study, to evaluate the cytotoxic effects of 5-ALA-PDT on FMT, 5-

ALA-HCl was added at final concentrations of 0, 0.03, 0.1, 0.3, and 1 mM (n = 3) and incubated for 4 h. The cells were irradiated with LED light of 633 nm wavelength at 20 mW/cm^2, 0, 5, 10, or 20 J/cm^2. The survival rate of the FKR cells was determined under these conditions. 5-ALA-PDT had a cytotoxic effect on FKR, and 5-ALA-PDT reduced cell survival in a PS dose-dependent manner. In addition, the cytotoxic effects of FKR-S cells were more substantial than those of FKR-A cells. Thus, the author evaluated the intracellular concentration of PpIX in FKR cells. The concentration of PpIX in FKR-S cells was approximately five-fold higher than that in FKR-A cells (P<0.05).

The cytotoxic potential of 5-ALA-PDT was assessed using mRNA expression levels of transporters associated with the uptake of 5-ALA and enzymes related to porphyrins metabolism and excretion. The target genes were divided into four major categories for analysis, based on ALA uptake transporter gene, genes related to heme synthesis, porphyrin excretion transporter, and hypoxia-related genes. About the 5-ALA uptake transporter gene, compared with FKR-A, FKR-S tended to have higher expression levels of the 5-ALA uptake transporter genes *PEPT1*, *PEPT2*, *GAT2*, and *TAUT*. Of these, the difference in the expression levels of *PEPT1* and *PEPT2*, which are mainly responsible for 5-ALA uptake, was most pronounced in FKR-S cells. About the genes related to heme synthesis, compared with those in FKR-A, the expression levels of *ALAS1* and *HO-1* tended to be higher in FKR-S, and the expression of *FECH* and *UROS* tended to be lower. About the porphyrin excretion transporter gene, in FKR-S, the expression level of *ABCG2* remained almost unchanged compared with that in FKR-A, and the expression of *ABCB6* was approximately half of the expression of FKR-A *ABCB6* mRNA. About the hypoxia-related genes, compared with those in FKR-A cells, the expression levels of *HIF-1α*, *LDHA*, and *LDHB* were not considerably altered in FKR-S cells. However, we observed

a trend toward enhanced expression of *PDK1*, which suppresses the activity of *PDH* and *VEGF*. The intracellular concentration of PpIX in FMT cells may be correlated with cell culture morphology (2D adherent and 3D spheroid cultures) and gene expression levels, including *PEPT1*, *PEPT2*, *FECH*, and *HO-1*.

In addition, FKR-S cells were subcutaneously inoculated into the backs of eight 6-week-old females NOD/ShiJic-scidJcl mice. When the average tumor volume reaches approximately 100 mm^3, four mice in the experimental group were intraperitoneally injected with 250 mg/kg 5-ALA-HCl, followed by PDT after 4 h. *In-vivo* findings showed that FKR-S tumor volume was reduced (from an average of 100.6 mm^3 to an average of 27.3 mm^3) after 24 h, after receiving one treatment of 5-ALA-PDT compared with the control group; tumor growth was subsequently inhibited.

In summary, *in vitro* cytotoxicity was correlated with PpIX concentration in FMT cells, and PpIX accumulation was correlated with differences in cell culture morphology (2D or 3D cultured). 5-ALA-PDT inhibits the growth of FMT *in vivo*.

Most *in vitro* studies on 5-ALA-PDT were conducted using 2D cultured cells due to the preparation simplicity and low maintenance and monitoring costs. Previous *in vitro* experiments using 2D culture did not reflect the *in vivo* condition, but it was thought that using 3D culture could produce results that reflect the *in vivo* condition. To our knowledge, this is the first study of 5-ALA-PDT using 3D-cultured primary FMT cells. By advancing the findings of this study, it may be possible to establish a less invasive treatment for mammary tumors in elderly cats.

CHAPTER1

General introduction

1.1. Feline Mammary Tumor (FMT)

1.1.1. Epidemiological

Feline mammary tumor (FMT) is a very common tumor in veterinary medicine, accounting for 17% of tumors in female cats [1]. The malignancy rate of FMT has been reported to be 80-90% [2], with a higher incidence in the abdominal gland sand a high rate of metastasis occurring in cases [3,4], and metastasis most often occurs in the regional lymph nodes and lungs [3–6]. FMT shares anatomical, biological, and clinical characteristics with human breast cancer (HBC), but the mechanism of metastasis is still poorly understood [7]. It is also classified into several molecular subtypes, including triple-negative normal basal-like, luminal A, luminal B, and epidermal growth factor receptor 2-positive (HER2-positive) [5,8]. Although the etiology is unknown, it is widely believed to be due to multiple factors, with major risk factors including gender, breed, age and hormonal influences [4,9]. A case-control study reported a lower risk of mammary cancer in cats spayed before one year of age and a seven-fold higher proportion of cats with mammary tumors were unspayed compared to controls [10].

Felines typically have four sets of mammary glands, two of which are located in the thorax and two in the abdomen. Mammary tumors appear as a single or multiple subcutaneous nodule or mass within the mammary gland, which may exhibit mobile, isolated, or adhered characteristics, and also could be ulcerated, or present as cystic [11]. One study reported that 60% of felines present with multiple mammary masses in several glands ipsilaterally or bilaterally [4,8]. Since it is difficult to distinguish whether a FMT is benign or malignant, all nodules should be treated as potentially malignant.

1.1.2. Therapeutic methods and prognosis

Feline mammary tumors are generally treated with surgery, chemotherapy, hormone therapy and radiation therapy [12,13]. Whereas surgical excision remains the most widely accepted treatment for FMT, unilateral or bilateral radical mastectomy is recommended in order to prolong the disease-free interval [11,14]. However, the complication (include infection, dehiscence, seroma, *etc*) rate was 19.7% after undergoing unilateral mastectomy and 40.6% after undergoing bilateral mastectomy [14]. Given the aggressive metastatic behavior of FMT, consideration should also be given to removing any lymph nodes with cytological evidence of metastasis. Despite this, however, it has been shown that one-year postoperative survival remains low in feline patients treated with surgery alone [15].

To maximize survival time, systemic chemotherapy may be used as an adjunct to surgery in the treatment of mammary tumor [16,17]. However, sequelae such as vomiting, anorexia, diarrhea, lethargy, myelosuppression, and seizures are usually observed [16]. And radiation therapy is rarely used in the treatment of mammary tumors [13].

Overall, although conventional therapies do provide some benefits in terms of quality of life and survival time, newer treatment options are still necessary. As a result, photodynamic therapy, which selectively eliminates tumor cells and can be used in combination with other therapies, is coming into focus.

1.2. Photodynamic Therapy (PDT)

1.2.1. Background

Ancient Egyptian, Chinese, and Indian civilizations employed light with active chemicals to cure ailments, including vitiligo, psoriasis, and skin cancer more than 3,000 years ago [18]. Light has been used therapeutically for thousands of years [19, 20]. In research of the effects of dye acridine on infusoria more than a century ago in 1900, Oscar Raab, a German student working for Prof. Hermann von Tappeiner, noticed that the toxicity of acridine varied according to the degree of exposure to light and discovered that specific wavelengths were lethal to infusoria [21]. The same year, French neurologist Jean Prime discovered that epileptic patients on oral eosin caused dermatitis in sun-exposed areas [21,22]. Later, in 1903, Hermann von Tappeiner and Albert Jesionek treated skin cancers using topical eosin and white light treatment [21–23]. Hermann Von Tappeiner looked into Oscar Raab's discoveries on the effects of the dye acridine on infusoria in more detail, creating the phrase "photodynamic action" [21,24]. Hematoporphyrin, the porphyrin presents in hemoglobin, and Friedrich Meyer-Betz performed a self-skin test, he noticed swelling and discomfort in the areas exposed to light [25]. Subsequent research with a hematoporphyrin derivative (HPD) by Lipson [26] demonstrated that the substance accumulates and fluoresces in tumors. It was a helpful diagnostic tool because of these characteristics and the lower dosage compared to crude hematoporphyrin [26]. A decrease in glioma development was noted for many weeks following HPD treatment before deeper tumor tissue started to recover, as demonstrated by Diamond et al. ten years later in their demonstration of the efficacy of HPD in treating cancer in mice [27]. The development of photodynamic treatment (PDT) in the 1970s was made possible by the work of Dougherty et al. First, they used HPD in conjunction with red light to completely

eradicate breast cancers in mice [28]. The first attempt to use PDT in the treatment of bladder cancer was made in 1970s, and other studies have been conducted on skin and lung tumors, with results showing effective control of cancer growth [29–31].

1.2.2. Principle and mechanism of PDT

Photodynamic therapy is the use of specific wavelengths of light irradiation of the target site, which uses photosensitizers and oxygen molecules and other conditions to generate reactive oxygen species (ROS), especially hydroxyl radical (HO) and singlet oxygen ($^1O_2$) [32] to induce apoptosis and necrosis [33], to achieve tumor growth inhibition [33]. As an emerging noninvasive treatment method, PDT has the advantages of less tissue trauma, low toxicity and no drug resistance compared to traditional treatments, and thus has received extensive attention from researchers in recent years [34]. Three conditions are required to achieve PDT: photosensitizer (PS), light, and oxygen. These three conditions are non-toxic when used alone. Still, the simultaneous action of the three can produce photochemical reactions, generating highly reactive and toxic ROS, including singlet oxygen, superoxide anion, hydroxyl radical, *etc*. Reactive oxygen species can cause apoptosis or necrosis, thus killing tumor cells [35,36]. The short half-life and strong reactivity of ROS and owing that only cells near the ROS-generating region (photosensitizer-localized region) are directly affected by PDT [37] theoretically make PDT specific and controllable.

The mechanism of PDT can be broadly classified into three categories: killing the tumor cells, destroying the vasculature, and triggering the body's immune response [38,39]. First, when the photosensitizer accumulates in the cell, PDT can be targeted according to the amount of intracellular photosensitizer accumulation, and the generated

ROS may lead to cell death, apoptosis, necrosis, and autophagy [40]. The cell-killing effect depends mainly on the concentration and distribution location of $^1O_2$ produced during treatment [41–43]. Second, the $^1O_2$ created by the photochemical reaction can damage the blood vessels when the photosensitizer is exposed to a laser while it is mostly localized within and around in blood vessels [44–46]. This will result in inadequate blood flow to the lesion and will indirectly cause cell death. Third, the locally induced acute inflammatory response during PDT and the later series of immune responses also have sustained systemic effects on tumor suppression and destruction [47–49].

1.2.3. PDT at a cellular level

The cellular damage caused by PDT mainly depends on the selective accumulation of the photosensitizer in subcellular structures such as cell membranes, mitochondria, lysosomes, and other organelles and the direct oxidative damage to these organelles leading to cell death [50]. Furthermore, three primary mechanisms of cell death are induced by PDT: apoptosis, necrosis, and autophagy.

Among them, apoptosis is a controlled cell death mechanism with highly regulated processes [51]. Following damage to a range of organelles caused by PDT, it can be started via various pathways [52]. PDT likely leads to apoptosis when PS accumulates mainly in mitochondria [53].

Secondly, higher PS doses and laser intensities exacerbate cellular damage. With extensive cellular damage, apoptosis is not executed correctly due to the absence of components of the apoptotic pathway, leading to necrosis rather than apoptosis [41–43]. In addition, necrosis rather than apoptosis is also more likely to be observed when the site of action of PS is the plasma membrane.

Finally, damaged and ruptured cell or organelle fragments are phagocytosed through cellular autophagy, which may act as a cytoprotective mechanism when lower doses of PS or weaker laser intensity cause less damage to cells [54]. Conversely, when cells are severely damaged, leading to apoptosis, autophagy may act as a cell-death mechanism to respond to PDT [55,56], becoming one of the leading causes of cell death [57,58].

1.3. Photosensitizer (PS)

1.3.1. 5-Aminolevulinic acid (5-ALA)

As a synthetic precursor of protoporphyrinic organisms, the second-generation photosensitizer 5-aminolevulinic acid (5-ALA) has been one of the research hotspots in the field of photodynamic therapy in the last few years, which is not entirely photosensitizing. It can be converted into the photosensitizer protoporphyrin IX(PplX) in cells [59]. The synthesis and degradation of PpIX, the immediate precursor of heme, is strictly monitored and maintained at low cell levels during normal physiological conditions [60]. Heme biosynthesis consists of a series of enzyme-catalyzed steps, the last of which is the conversion of PpIX to heme using ferrochelatase (*FECH*) located in the inner mitochondrial membrane [61]. Although 5-ALA synthesis is negatively feedback-regulated by ferrous heme, exogenous increases in 5-ALA will affect this feedback-regulatory system, accumulating PpIX. The red fluorescence emitted by PpIX when irradiated with visible blue light (375–475 nm), or the generation of cytotoxic substances when irradiated with specific wavelengths of red light (630 ± 5 nm), is the basis for photodynamic diagnosis (PDD) and PDT photosensitizing effects [62].

1.3.2. Generation pathway of photosensitizer protoporphyrin IX (PplX)

Protoporphyrin IX is an endogenous photosensitizer with strong photosensitizing activity, which is irradiated by red light around 630 nm to produce ROS such as singlet oxygen ($^1O_2$). The singlet oxygen oxidatively damages the subcellular structures such as mitochondrial, cell membranes and lysosome, ultimately to the therapeutic effect [63,64]. In the cytoplasm, 5-ALA undergoes the porphobilinogen (*PBG*)–hydroxymethylbilane (*HMB*)–uroporphyrinogen III (*UROIII*)–coproporphyrinogen III (*COPROIII*) pathway,

forms PpIX in the mitochondria, and finally becomes heme, catalyzed by ferrochelatase (*FECH*) [65–67]. Notably, the first step in the heme synthesis pathway is the production of 5-ALA from the condensation reaction of glycine and succinyl-CoA catalyzed by the rate-limiting enzyme, 5-aminolevulinic acid synthase (*ALAS*), which occurs in mitochondria, where it is inhibited by heme feedback [68,69]. However, in the presence of exogenous 5-ALA, synthesis inhibition of synthesis is lifted, and the synthesis of the intermediate PpIX increases. Heme oxidase-1 (*HO-1*) is also the rate-limiting enzyme for the synthesis of heme. treatment with ALA or PpIX leads to enhanced mRNA expression of *HO-1*, which metabolizes heme to biliverdin, carbon monoxide, and ferrous iron and dose-dependently inhibits mRNA expression of *ALAS1* [65]. In addition to enzymes, various transporter proteins are involved in producing and disposing of PpIX. Fecal porphyrinogen III is transported from the cytoplasm back to the mitochondria by ATP-binding cassette transporter protein subfamily B member 6 (*ABCB6*), found in the outer mitochondrial membrane. Here, it completes the final three stages of heme production [70,71]. In cell membranes and mitochondrial cristae, ATP-binding cassette transporter protein subfamily G member 2 (*ABCG2*) is expressed [72,73]. The primary route for PpIX elimination in the body is via hepatocyte uptake and excretion into the bile ducts, which is facilitated by *ABCG2*'s pumping of PpIX from myeloid cells and erythrocytes into the plasma [74–78]. It can be seen that the expression of relevant genes and proteins has a crucial effect on the accumulation of PpIX [79], so when the cell morphology is altered and results in differences in the expression of genes and proteins [80,81], it is hypothesized that the accumulation of PpIX will also change.

1.4. Two-dimensional (2D) and Three-dimensional (3D) Cell Cultures

1.4.1. 2D cell cultures

The most used tumor cell culture method in studies related to PDT is still the 2D model culture. In adherent 2D culture, cells grow as a monolayer attached to a surface in a culture flask or flat dish [82].

2D culture mainly has the advantages of simplicity of cell culture, low maintenance costs, and the ability to fulfill essential research testing functions. However, with the depth of various studies, the disadvantages of 2D culture have been gradually exposed. Firstly, under the conditions of 2D culture, tumor cells grown adherent to the flat surface on a flask or plate cannot mimic the natural structure of cellular tissues or tumors [83–85]. As a result, the interactions between cell–cell and cell–extracellular matrix (ECM) could not be fully expressed as in tumor tissues. These interactions affect cell proliferation, differentiation, gene and protein expression, drug metabolism and other cellular functions, and response to external stimuli [86–89]. Upon isolation from tissues and transfer to 2D conditions, the morphology of the cells is altered, and the pattern of cell division is changed. The loss of diverse phenotypes is also a result of 2D culture [90,91]. Altered cell morphology affects its function, the organization of intracellular structures, secretion, and cell signaling [90–92]. In addition, alien to the *in-vivo* tumor microenvironment, due to the monolayer nature of 2D cultures, all cells in the culture receive equal amounts of oxygen, nutrients, and drugs [86,93]. Oxygen concentration and the uptake of externally given photosensitizer by tumor cells are key factors affecting the therapeutic efficacy of 5-ALA-PDT, leading to the need for more suitable tumor cell culture models to enhance the accuracy of *in vitro* studies.

1.4.2. 3D cell cultures

Due to the shortcomings of 2D cultures, three-dimensional (3D) in vitro models have gained increasing momentum in drug screening and tumor research owing to their improved ability to recapitulate the complexity of the tumor microenvironment (TME) [94,95]. The use of 3D culture models for PDT studies also has developmental implications that can improve the predictability of toxicity and drug sensitivity in cancer [96].

To create one of the first 3D primary organoid cultures in the field of mammary tumor research, researchers cleverly combined 3D cultures in collagen gels [97] or laminin-rich gels [98] with a protocol for the isolation of primary mammary epithelial tissue fragments that was proposed nearly 50 years ago [99]. Nowadays there are three different methods of preparing 3D culture models: suspension cultures on non-adherent plates, cultures in concentrated medium or in gel-like substances and cultures on a scaffold [91].

The 3D culture of tumor cells comprises cells forming individual layers that combine to form a spherical structure. This structure largely mimics solid tumor tissues' physical and biochemical characteristics, similar to cells grown in vivo in terms of cell topology, gene expression, signaling, and metabolism [100–102], facilitating cell-cell and extracellular matrix (ECM) interactions. This structure allows cells to receive stimuli from the local environment as *in vivo* [103,104]. Furthermore, since changes in ECM composition correlate with cancer progression and tumor characteristics [105], ECM interactions play an essential role in tumor drug resistance, in which case 3D culture could open the door to better preclinical screening of drug candidates [106,107].

1.5. Objectives of this study

1. The mortality rate of 5-ALA-PDT-induced primary homologous feline mammary tumor cells in 2D and 3D culture conditions was determined by measuring cellular ATP with a luminescence photometer for effect evaluation.

2. qRT-PCR was used to determine the expression of relevant mRNAs and to investigate the reasons for the differences in the therapeutic effects induced by 5-ALA-PDT at the molecular level.

3. *In vivo* assays were performed to assess the efficacy of 5-ALA-PDT in feline mammary tumors.

CHAPTER2

In vitro evaluation of the efficacy of photodynamic therapy using 5-ALA on homologous feline mammary tumors in 2D and 3D culture conditions and a mouse subcutaneous model with 3D cultured cells

2.1. Introduction

Feline mammary tumors (FMTs), similar to those in people, are among the most frequent causes of cancer-related mortality in female cats [108,109]. FMTs may serve as cancer models because they exhibit molecular, histological, epidemiological, and clinicopathological classifications similar to those reported in human breast cancer. [109–111]. However, the antitumor effects of 5-ALA-PDT on FMT remain unclear.

Primary FMT FKR-A (two-dimensional [2D] culture) and FKR-S (three-dimensional [3D] culture) cells are established cell lines to explore FMT treatment *in vitro*. FMT FKR cells were isolated and cultured from the mammary tumor tissue of a 14-year-old spayed female mongrel cat. The 2D adherent proliferating cells were FKR-A cells, and the 3D spheroid proliferating cells were FKR-S cells, and each cell was passaged and maintained. Notably, in this study, the original FKR-A and FKR-S cells were derived from the same tumor tissue. Importantly, the 3D-cultured FKR-S cells that more accurately recapitulate physiological conditions are naturally formed when FKR-A cells are cultured. With cell culture passaging, some FKR-A cells will naturally form FKR-S cells when the number of cells increases, and there is insufficient space for growth, and vice versa. In this study, the spherical structures observed in the experimental group of FKR-S cells are not individual cells but spherical cell clusters made up of aggregates of unequal amounts of individual cells. As the spherical cell clusters vary considerably in size, quantitative analyses among the individual clusters were not performed in this study.

This study aimed to evaluate the therapeutic effect of 5-ALA-PDT in FMTs through *in vitro* experiments using FKR-A and FKR-S cells. Currently, 3D cultures are less commonly used than are mainstream 2D cultures in *in vitro* studies. Therefore, the present study also assessed the effect of differences in culture methods on 5-ALA-PDT for FMTs,

with the aim of advocating the use of suitable culture methods to establish *in vitro* biological models that more closely resemble the environment in living organisms. This included the comparative determination of cell viability between FKR-A and FKR-S cells, determination of intracellular PpIX content, assessment of cell death, and determination of 5-ALA uptake transporter genes, heme synthesis-related genes, and porphyrin excretion transporter genes. In addition, because FKR-A and FKR-S cells are inherently homologous tumor cells (FKR cells), with the only difference being the number of cell passages *in vivo*, mice were inoculated with FKR-S cells only for *in vivo* studies to evaluate the *in vivo* inhibitory effect of 5-ALA-PDT on FMT FKR cells.

2.2. Materials and methods

2.2.1. Materials

SBI Pharmaceuticals Co., Ltd. (Tokyo, Japan) donated 5-ALA hydrochloride (5-ALA-HCl).

2.2.2. Cells

We successfully established homologous FMT cells, named FKR cells. These cells were cultured at 37°C with 5% CO_2. RPMI 1640 medium was supplemented with 5 mg/mL streptomycin, 5 mg/mL penicillin, 10 mg/mL neomycin (Invitrogen; Thermo Fisher Scientific, Inc.), and 10% heat-inactivated fetal bovine serum (FBS; Nichirei Biosciences Inc. in Tokyo, Japan).

2.2.3. Cell viability

We seeded 2×10^4 2D-cultured FKR cells (FKR-A cells) and 3D-cultured FKR cells

(FKR-S cells) into each well of white 96-well plates (Corning Inc, Armonk, NY, USA) and incubated the cells at 37°C for 24 h. The cells were then washed twice with phosphate-buffered saline (PBS) and a fresh medium was added. Next, 5-ALA-HCl was added at final concentrations of 0, 0.03, 0.1, 0.3, and 1 mM (n = 3) for 4 h. After being washed with fresh medium, the cells were exposed to 633-nm wavelength radiation from an LED light (Pleiades Technology LLC., Fukuoka, Japan) at 20 mW/cm^2, 0, 5, 10, and 20 J/cm^2. The cells were then incubated at 37°C for 24 h in the dark. The amount of ATP was determined using luminescence photometry (LuMate Microplate Luminometer, Awareness Technology Inc., Palm City, FL, USA) using the KATAMARINO ATP assay reagent ver.2 (Toyo Benet Co., Ltd., Tokyo, Japan), following the manufacturer's directions. ATP is an important source of cellular energy [112], and the amount of intracellular ATP is related to cell viability and can indicate the number of viable cells.

2.2.4. Evaluation of cell death

FKR-A and FKR-S cells were cultured in clear 96-well plates (Corning Inc.) using the cell culture method mentioned in section 2.2.3. Subsequently, 5-ALA-HCl was added to achieve final concentrations of 0, 0.3, and 1 mM, and cells were cocultured for 4 h. Subsequently, irradiation with a 633-nm wavelength (20 mW/cm^2, 10 J/cm^2) emitted by the LED light was conducted. After PDT, the culture was continued for 24 h, and ethidium homodimer III (5 μL; EthD-III), annexin V, and Hoechst 33342 (Promo Kine production) were subsequently added to each well, respectively. The Apoptotic/Necrotic/Healthy Cells Detection Kit is a practical assay to identify healthy (blue), necrotic (red), and apoptotic (green) cells within the same cell population using fluorescence microscopy. After staining, the cell viability was observed under fluorescence microscopy (BZ-X810;

Keyence Co., Osaka, Japan).

2.2.5. Intracellular PpIX concentration in FKR-A and FKR-S cells

A 75-cm^2 tissue culture flask (Corning Inc.) was seeded with 1–2 × 10^6 FKR-A cells and incubated for 24 h. FKR-S cells (1 mL) were washed twice with PBS and then cultured in a 75-cm^2 culture flask. FKR-A and FKR-S cells were incubated with 0.3 and 1 mM 5-ALA-HCl for 4 h. Trypsin was used to separate the FKR-A cells from the culture flask after two PBS washes. FKR-S cells underwent two PBS washes. A total of 200 μL of centrifuged FKR-A and FKR-S cell solution were placed in 1.5 mL Eppendorf tubes, respectively, and then lysed by sonication for 30 s. The concentration of PpIX in FKR-A and FKR-S cells was determined according to a previous report [113].

2.2.6. Histological evaluation

A 75-cm^2 tissue culture flask (Corning Inc.) was seeded with 1.5–2 × 10^4 FKR-A cells and then incubated for 24 h. FKR-S cells (1 mL) were washed twice with PBS and then cultured in 75-cm^2 culture flasks (Corning Inc.). FKR-A and FKR-S cells were then incubated with 0.3 mM 5-ALA-HCl for 4 h. Trypsin was used to separate the FKR-A cells from the culture flask after two PBS washes; FKR-S cells underwent two PBS washes.

The cells were fixed in 4% buffered formalin. Next, samples were paraffin-embedded, sectioned to a thickness of 4 μm, and stained with terminal deoxynucleotidyltransferase-mediated dUTP nick end labeling (TUNEL) and hematoxylin and eosin (H&E). TUNEL staining was performed *in situ*.

2.2.7. mRNA expression

Cell culture was performed in the same way as mentioned in section 2.5. RNA levels were determined by qRT-PCR (triplicate) on the FI Step One PlusTM system using a SYBR Select Master Mix (Applied Biosystems®, Waltham, MA, USA). The mRNA expression levels in FKR-A and FKR-S cells were determined according to a previous report [114]. Target genes and specific primers used for each gene are listed in Table 1. mRNA sequences were selected according to previously described methods [115].

2.2.8. *In vivo* evaluation of the antitumor effect

Eight six-week-old female NOD/ShiJic-scidJcl mice (CLEA Japan, Inc., Tokyo, Japan) were housed in a Jic rack (Jic Co., Kanagawa, Japan) under sterile conditions and given unlimited access to gamma-sterilized food (CL-2; CLEA Japan) and autoclaved water. The Tottori University Animal Research Committee approved the use of animals and the methods in this study (project number: 19-T-31). The mice were divided into two cages, with four mice per cage. One group was the control group, and the other was the 5-ALA-PDT experimental group. A subcutaneous injection of 1–2 × 10^6 FKR-S cells/0.1 mL PBS was administered into the backs of all eight mice.

After approximately 2 weeks, when the average tumor volume reached approximately 100 mm^3, four mice in the experimental group were intraperitoneally injected with 250 mg/kg 5-ALA-HCl. Four hours later, they were irradiated with a 636-nm wavelength (250 mW/cm^2, 150 J/cm^2) emitted by a diode-pumped solid-state laser (HangZhou NaKu Technology Co. Ltd, Zhejiang, China). Continuous measurement of tumor volume was conducted in the mice over 2 weeks. Histopathological sections were obtained from the tumor tissues of the control and experimental groups. The experiment was terminated on day 14.

The mice were euthanized by cervical dislocation, and the tumors were harvested 24 h after 5-ALA-PDT administration, to examine the PDT-induced histological changes in the tumor tissue. Tumor tissues were fixed in 4% buffered formalin. The specimens were then embedded in paraffin, sectioned to a thickness of 4 μm, and stained with H&E and TUNEL.

2.2.9. Statistical analysis

Differences between the experimental groups were analyzed for statistical significance using the multiple paired *t*-test. Statistical significance was set at a p-value <0.05.

2.3. Results

2.3.1. Cell viability

We measured the cell survival rate, as shown in Fig. 2a. When no light irradiation was performed (20 mW/cm^2, 0 J/cm^2), the number of both types of tumor cells showed a slow decreasing trend. However, when the light fluence rate was 20 mW/cm^2 and light fluence was 5 J/cm^2 (Fig. 2b), the FKR-S cell viability decreased to 2.79% at 0.3 mM 5-ALA-HCl.

When the light fluence rate was 20 mW/cm^2 and light fluence was increased to 10 J/cm^2 (Fig. 2c), the viability in both FKR-A and FKR-S cells significantly decreased. At 0.3 mM 5-ALA-HCl, the FKR-S cell viability dropped sharply to 4.69% compared with that at 0 mM 5-ALA-HCl, while FKR-A cells were also in a nodal position, reaching a low viability of 49.97% compared with that at 0 mM 5-ALA-HCl. Cell viability also significantly decreased ($p<0.01$) at 1 mM 5-ALA-HCl; however, in general, the decrease

was far less significant than that at 0–0.3 mM 5-ALA-HCl (0.81% for FKR-S cells and 38.08% for FKR-A cells). Meanwhile, the FKR-S cell viability was lower than that in FKR-A cells under the same conditions. A similar result was observed when the light fluence rate was 20 mW/cm^2 and light fluence was 20 J/cm^2 (Fig. 2d).

2.3.2. Evaluation of cell death

To observe the extent of cell death in FKR-A and FKR-S cells, the cells were incubated with two different concentrations (0.3 and 1 mM) of 5-ALA-HCl for 4 h and then irradiated. After 24 h, the cells were stained with Hoechst 33342, EthD-III, and annexin V and observed under fluorescent microscopy (Fig. 3).

The degree of necrosis and apoptosis in both FKR-A and FKR-S tumor cells increased with increasing 5-ALA-HCl concentrations.

In FKR-A cells, green-stained areas, representing apoptotic cells, increased significantly with increasing 5-ALA-HCl concentrations, and the number of stained cells increased (Fig. 3a). The amount of red staining, representing necrotic cells, greatly increased at 1 mM 5-ALA-HCl compared with that at 0 and 0.3 mM 5-ALA-HCl. The area of live-cell staining in FKR-A cells far exceeded the areas of apoptotic and necrotic staining at 0 and 0.3 mM 5-ALA-HCl. At 1 mM 5-ALA-HCl, no evident difference was visualized between individual staining areas.

In FKR-S cells, the area of green staining, representing apoptosis, and the number of cells did not change with increasing 5-ALA-HCl concentrations (Fig. 3b). However, FKR-S cells manifested a large red area, representing necrosis, at 0, 0.3, and 1 mM 5-ALA-HCl. As shown in the composite graph, there was no obvious difference between the necrotic- and live-stained areas in FKR-S cells at 0 mM 5-ALA-HCl. At 0.3 mM

5-ALA-HCl, the stained area of living cells was larger than that of necrotic cells. At 1 mM 5-ALA-HCl, the stained area of the living cells included necrotic and apoptotic areas.

2.3.3. Intracellular PpIX concentration in FKR-A and FKR-S cells

Most porphyrins detected in the cells and culture supernatants were PpIX. The amount of PpIX in the cells was approximately 5-fold higher in the 3D culture of FKR-S cells than in the 2D culture of FKR-A cells (Fig. 4a). The amount of PpIX in the culture supernatant tended to be higher in the 2D cultures but the difference was smaller than that of the amount of PpIX in the cells (Fig. 4b). When the concentration of 5-ALA-HCl increased by 3.3-fold, the amount of PpIX that accumulated in the cells increased by approximately 1.3-fold. This trend remained the same for the FKR-A and FKR-S cells.

2.3.4. Histological evaluation

The number of FKR-A cells (Fig. 5a–d) decreased after 5-ALA-PDT. Cells treated with 5-ALA-PDT were shrunken (Fig. 5c) and stained slightly with TUNEL (Fig. 5d). In FKR-S cells (Fig. 5e–h), the cells within the spheroids were stained slightly with TUNEL prior to 5-ALA-PDT (Fig. 5f). Spheroid cells shrank (Fig. 5g), and the number of TUNEL-positive cells increased (Fig. 5h) after 5-ALA-PDT.

2.3.5. mRNA expression

The target genes were divided into four major categories for analysis, based on ALA uptake transporter gene, genes related to heme synthesis, porphyrin excretion transporter, and hypoxia-related genes. The target genes and specific primers for each gene are shown

in Table 1.

2.3.5.1. 5-ALA uptake transporter gene

Compared with FKR-A, FKR-S tended to have higher expression levels of the 5-ALA uptake transporter genes *PEPT1*, *PEPT2*, *GAT2*, and *TAUT* (Fig. 6). The relative quantitative value of mRNA expression (normalized to *ACTB*) in FKR-A cells was taken as 1, and the following results of mRNA expression were applied. Of these, the difference in the expression levels of *PEPT1* and *PEPT2*, which are mainly responsible for 5-ALA uptake, was most pronounced in FKR-S cells. The expression of *PEPT1* in FKR-S cells was approximately 2.5-fold that of FKR-A cells, whereas the expression of *PEPT2* was approximately 5-fold that of FKR-A cells. The expression of *TAUT* was approximately 1.88, and that of *GAT2* was 1.30.

2.3.5.2. Genes related to heme synthesis (heme synthase)

The expression of *ALAS1* mRNA in FKR-S cells was approximately 1.58 and the expression of *HO-1* mRNA was approximately 4.26 (Fig. 7), while the expression of *FECH* mRNA was approximately 0.45, and the expression of *UROS* mRNA was approximately 0.54. It can be observed that compared with those in FKR-A, the expression levels of *ALAS1* and *HO-1* tended to be higher in FKR-S, and the expression of *FECH* and *UROS* tended to be lower.

2.3.5.3. Porphyrin excretion transporter gene

In FKR-S, the expression level of *ABCG2* remained almost unchanged compared with that in FKR-A (Fig. 8). The expression of *ABCG2* in FKR-S was approximately 1.08; the expression of *ABCB6* was approximately 0.57, which was approximately half of the

expression of FKR-A *ABCB6* mRNA.

2.3.5.4. Hypoxia-related genes

Compared with those in FKR-A cells, the expression levels of *HIF-1α*, *LDHA*, and *LDHB* were not considerably altered in FKR-S cells (Fig. 9). However, we observed a trend toward enhanced expression of *PDK1* (pyruvate dehydrogenase kinase 1), which suppresses the activity of pyruvate dehydratase (*PDH*) and vascular endothelial growth factor (*VEGF*). The expression of *PDK1* in FKR-S was approximately 2.76, while that of *VEGF* was approximately 1.51.

2.3.6. *In vivo* evaluation of the antitumor effect

Figure 10 shows that the volume of the tumor tissue treated with 5-ALA-PDT was significantly lower than that of the untreated control group.

Moreover, the volume of the tumor tissue gradually increased over time in the untreated control group, reaching 270.7 mm^3 on day 14, which was 306% of that on day 0. In contrast, the group treated with 5-ALA-PDT showed a considerable decrease in tumor tissue volume after 24 h of PDT, from an average of 100.6 mm^3 to an average of 27.3 mm^3. Although a small rebound occurred daily thereafter, the tumor tissue volume on day 14 remained smaller than that before treatment, averaging 95.1 mm^3.

2.3.7. Histological examination

In untreated tumor tissues (Fig. 11a, b), necrotic areas were observed in the center of the tumors, and the boundary between the tumor and necrotic tissues was clearly defined.

In the treated tumor tissues (Fig. 11c, d), the tumor cells appeared necrotic and

apoptotic. Pyknosis and cell separation were observed; however, the boundary between the tumor and necrotic tissues was unclear.

2.4. Discussion

In the present study, we evaluated the cytotoxic and antitumor effects of 5-ALA-PDT on FMT FKR-A and FKR-S cells and the mRNA expression levels associated with PpIX accumulation. To our knowledge, this is the first study of 5-ALA-PDT using naturally occurring 3D FMT cells.

In vitro cell culture methods (2D), in contrast to 3D culture, involve conventional uses of flat supports [116,117] for cell development in monolayers. However, this culture method cannot perfectly replicate physiological settings and the natural microenvironment, including the tissue structure, physiology, biological signals of live tissues, and interactions between cells and the matrix, resulting in several limitations [117–122]. In addition, differences in gene expression levels between 2D and 3D cultures of mammary tumor cells have implications for drug screening. Cellular 3D cultures have been shown to better recapitulate the tumor response to anticancer drugs than 2D cultures [123,124]. These include changes in the expression of genes related to drug metabolism, transporters, and survival pathways. Therefore, 3D models provide more accurate predictions of drug efficacy.

In vitro evaluation: Accordingly, we used both 2D and 3D culture methods to study the effect of 5-ALA-PDT on FMT. Our results showed that the concentration of intracellular PpIX in 3D-cultured FKR-S cells was approximately 5-fold higher than that in 2D-cultured FKR-A cells at the same dose of 5-ALA (Fig. 4). Similarly, the cytotoxicity induced by 5-ALA-PDT was higher in FKR-S cells than that in FKR-A cells, which

correlates with the cytotoxicity assay results (Fig. 2). Based on the cytotoxicity assay results, 5-ALA-PDT reduced cell viability in a dose-dependent manner. That is, the higher the 5-ALA concentration and light intensity, the lower the cell survival rate. In particular, the cell survival rate was most significantly reduced at 0.3 and 1 mM 5-ALA. Our findings demonstrate that 5-ALA-PDT has an inhibitory or even cytotoxic effect on FKR-A and FKR-S cells. Histological evaluation showed that FKR-A and FKR-S cells treated with 5-ALA-PDT underwent degeneration (Fig. 5). In addition, 5-ALA-PDT was more effective against FKR-S cells than against FKR-A cells. Therefore, we investigated the expression levels of various genes that may affect ALA-mediated PpIX accumulation in several tumor cell lines, including 5-ALA uptake transporter genes, porphyrin transporter genes, and heme synthesis-related genes (Figs. 6–9).

Based on our results, we confirmed that 2D-cultured FKR-A cells differed in gene expression levels from 3D-cultured FKR-S cells. Several studies have shown that the cellular microenvironment and culture conditions in 3D systems can significantly influence gene expression patterns. The *VEGF* expression level was higher in 3D-cultured FKR-S cells than that in 2D-cultured FKR-A cells (Fig. 9). According to other studies, tumor microenvironment (TME) cells promote angiogenesis by secreting *VEGF* and fibroblast growth factor 2 (*FGF-2*) [125], and the newly created capillaries feed the expanding tumor tissue with oxygen and nutrients.

The present study showed that the expression levels of both *PEPT1* and *PEPT2* were higher in FKR-S cells (Fig. 6). From a medicinal chemistry perspective, the uptake of 5-ALA into transgenic yeast cells expressing the mammalian di- and tri-peptide transporters *PEPT1* and *PEPT2* suggests that these systems contribute to the delivery of 5-ALA [126]. Furthermore, the 5-ALA influx transporters *PEPT1* and *PEPT2* are extensively expressed

in tumor cells, leading to increased PpIX accumulation [127–129]. Thus, the high expression levels of *PEPT1* and *PEPT2* in FKR-S cells may result in a large influx of 5-ALA into the tumor cells.

An ATP-binding cassette (*ABC*) transporter G2 (*ABCG2*) has been implicated in the regulation of the intracellular accumulation of porphyrin derivatives in tumor cells, which excrete excess PpIX from tumor cells and reduce the therapeutic efficacy of PDT [130,131]. However, in FKR-S cells with better PDT efficacy, the expression level of *ABCG2* was marginally higher than that in FKR-A cells (Fig. 8); these results contrast with those of previous reports [132,133], which have not yet been fully resolved due to the multitude of factors affecting PDT by *ABCG2*. We considered that the overall intracellular PpIX content was not reduced because of the possibility that excess PpIX released by the cells was reabsorbed by the surrounding cells. In mitochondria, CPGIII is converted to protoporphyrinogen (Ppgen), which is then converted to PpIX; *ABCB6* can mediate the entry of fecal porphyrinogen III into mitochondria [130,132], excluding excess fecal porphyrinogen III from tumor cells, which is the same as that of *ABCG2* and PpIX. The results showed that the expression of *ABCB6* was lower in FKR-S cells, which had a stronger effect of PDT.

FECH, *HO-1*, and *ALAS1* are intracellularly involved in heme synthesis. The results of this study showed that the expression level of *FECH* was two-fold different between FKR-A and FKR-S cells (Fig. 7). Iron (Fe^{2+}) is incorporated into PpIX via *FECH* to form heme, thereby reducing the level of PpIX available for PDT [133]. However, other studies have shown that the Warburg effect, where the tricarboxylic acid cycle is downregulated, results in a shortage of electrons necessary to decrease ferric ions to ferrous ions since anaerobic metabolism in cancer cells is greater than that in normal cells [134,135]. This

leads to a decline in *FECH* activity, which transforms PpIX into heme. As a result, PpIX preferentially accumulates in cancer cells [134]. As previously mentioned, the low expression of *FECH* favors the selective accumulation of PpIX in 3D-cultured FKR-S cells, thereby enhancing the therapeutic efficacy of 5-ALA-PDT. However, the accumulation of PpIX in tumor cells is influenced by multiple interacting factors, and several studies have shown that *HO-1* expression reduces PpIX accumulation [136,137] and exerts a protective effect against PDT-mediated cytotoxicity [138]. This could not explain why *HO-1* expression in FKR-S cells with stronger PDT effects in the present study was up to 4 times higher than that in FKR-A cells with weaker PDT effects (Fig. 7); thus, the mechanism of *HO-1* expression in cat mammary tumor cells, FKR cells, required investigation.

The crucial enzyme, 5-aminolevulinate synthase (*ALAS*), enables the production of 5-ALA from glycine and succinyl-CoA and is the first rate-limiting enzyme [139]. Negative feedback mechanisms via *ALAS1* inhibition by excessive heme rigorously regulate heme production in non-erythrocytes by reducing transcription and translation, destabilizing mRNA, inhibiting mitochondrial transport of precursor proteins, and degrading precursor proteins [140]. Combined with the higher expression of *ALAS1* in FKR-S cells than that in FKR-A cells in the present study (Fig. 7), this indicates that hemoglobin production in 3D-cultured FKR-S cells is lower than that in 2D-cultured FKR-A cells and further explains the diminished conversion of PpIX to hemoglobin by reduced *FECH* activity.

These results suggest that the high expression levels of *PEPT1*, *PEPT2*, and *ALAS1* in FKR-S cells, synergized with the low expression levels of *ABCB6* and *FECH* and other synergistic effects, lead to a strong accumulation of intracellular PpIX, ultimately

resulting in a stronger effect of PDT than that in FKR-A cells. These findings suggest that the uptake mechanisms of 2D cells and 3D spheroids may differ, even for homologous tumor cells.

In vivo evaluation: In the present study, we evaluated the inhibitory effect of 5-ALA-PDT on FKR-S tumor cells *in vivo*. Since FKR-S and FKR-A cells are essentially homologous and tumor cells do not grow in a monolayer *in vivo*, and FKR-A cells will autogenously grow into FKR-S cells in a 3D state after transplantation into mice through passaging, only FKR-S cells were used in this *in vivo* assay. According to the results of *in vivo* studies, the average tumor volume after a single 5-ALA-PDT session was 35.13% of that in the control group (No 5-ALA-PDT performed), which has a significant inhibitory effect (Fig. 10). The mean tumor volume after 24 h of a single 5-ALA-PDT treatment was reduced to 27.14% of the pre-PDT volume, and although the tumor volume continued to increase over the next two weeks, it remained lower than the pre-PDT volume, which was approximately 94.51% of the pre-treatment volume (Fig. 10). Histological examination also revealed a large number of necrotic cells after PDT (Fig. 11), indicating that a single 5-ALA-PDT session could have an inhibitory effect on the continued development of mammary tumors in NOD/ShiJic-scidJcl mice.

Multiple studies have shown that 5-ALA-PDT is effective against human and canine mammary tumors [114,141–143], and we verified, for the first time, the inhibitory and cytotoxicity effects of 5-ALA-PDT on primary cultured FMT FKR cells. Based on *in vitro* studies, we demonstrated that the effects of 5-ALA-PDT on homologous FMTs exhibited a significant difference in 2D and 3D cultures. In the present study, we assessed, as far as possible, the possible reasons for this disparity due to differences in the expression levels of the genes involved; however, differences in the TME during 2D and

3D culture remain to be investigated.

2.5. Conclusions

The results of this study confirm the inhibitory effect of applying photodynamic methods in FKR cells in FMTs. However, although FKR-A and FKR-S are derived from the same tumor tissue, the effects obtained in *in vitro* studies can vary due to differences in the TME and culture morphology (2D and 3D cultures). The expression levels of *PEPT1*, *PEPT2*, *HO-1*, and *FECH* mRNAs closely correlated with PpIX accumulation. Furthermore, 5-ALA-PDT inhibited tumor growth of FKR-S cells in FMTs *in vivo*.

Table 1. Target genes and specific primers for each gene.

Target genes	
ALA uptake transporter gene	*PEPT1*, *PEPT2*, *GAT2*, *TAUT*, *PAT1*
Genes related to heme synthesis	*ALAS1*, *ALAD*, *HMBS*, *UROS*, *UROD*, *GAPDH*, *CPOX*, *PPOX*, *FECH*, *HO-1*
Porphyrin excretion transporter gene	*ABCG2*, *ABCB6*
Hypoxia-related genes	*HIF-1α*, *LDHA*, *LDHB*, *PDK1*, *VEGF*

Primer	Sequence	Primer	Sequence
PEPT1	Fw: cagaagccagaaaaaggagaaa	*PEPT2*	Fw: ccacctcctgaaggaaacatag
（XM_023252783.1）	Rv: aaaactgatattcgctggcatt	（XM_003991691）	Rv: agctgctttgggtatttctcag
GAT2	Fw: ttctcattctcagcgtgtctgt	*TAUT*	Fw: gatcgactttgtgctctctgtg
（XM_023256642）	Rv: atggcctgtacccaatcatatc	（XM_003982523）	Rv: ggccaggatgatgacgtagtat
PAT1	Fw: ggtggacttcttcctgattgtc	*ALAS1*	Fw: atgagtttggagcaatcacctt
（XM_006927971）	Rv: gtctcattgttgtggcagttgt	（XM_003982295）	Rv: atgtccattttgggcataactc
ALAD	Fw: tgtgtaccacgtttctggagag	*HMBS*	Fw: ttgaaatcgttgctatgtccac
（XM_019816383）	Rv: ggcgtgtagtaggtgatgatga	（NM_001177808）	Rv: gggagtgaacgactaagtccac
UROS	Fw: tatggacttgaagccactctga	*UROD*	Fw: ttcccagagccattaagagaag
（XM_023241082）	Rv: acagctctctccttctgtgtcc	（XM_003990027）	Rv: gatatgggaccagagcatcagt
GAPDH	Fw: ctcatgaccacagtccatgc.	*CPOX*	Fw: tccatccaaggaagaagtgttt
（NM_001009307.1）	Rv: gtgagcttcccattcagctc	（XM_003991594）	Rv: cacagtgctttttcacaagagg
PPOX	Fw: ctggatgctgaccacgttatta	*FECH*	Fw: tggtcattctcttttctgctca
（XM_011291117）	Rv: gaaagcaaccgagtcatacaca	（XM_006938940）	Rv: ttcaatgtgatcgctggtaaac
HO-1	Fw: caggtcctcaagaagattgctc	*ABCG2*	Fw: tttcagggctgttggtaaatct
（XM_003989222）	Rv: gtacagctgcttgaacttggtg	（XM_023252947）	Rv: ttaccaaaaattcttcgccagt
ABCB6	Fw: attgtgttcctgtgcatgagtc	*HIF-1α*	Fw: cacatagaaatggccttgtgaa
（XM_003991168）	Rv: tttgacttccactccaaatcct	（XM_003987716）	Rv: tagacatgaatatggcctgtgc
LDHA	Fw: attggaagtggttgcaatctg	*LDHB*	Fw: agcgggtgtaatctggattct
（XM_019812152.2）	Rv: gggagacaccagcaacattta	（XM_003988487.3）	Rv: atgttctcccaaaatccatcc
PDK1	Fw: ccgtctcatcgaaaacacatt	*VEGF*	Fw: acgaagtggtgaagttcatgg
（XM_006935366.4）	Rv: ctgtcctggtgattttgcatt	（NM_001009854.1）	Rv: gcatggtgatgttgaactcct

Peptide transporter 1 (*PEPT1*), peptide transporter 2 (*PEPT2*), gamma amino butyric acid transporter 2 (*GAT2*), taurine transporter (*TAUT*), H+/amino acid transporter 1 (*PAT1*),

5'-aminolevulinate synthase 1 (*ALAS1*), aminolevulinate dehydratase (*ALAD*), hydroxymethylbilane synthase (*HMBS*), uroporphyrinogen III synthase (*UROS*), uroporphyrinogen III decarboxylase (*UROD*), glyceraldehyde-3-phosphate dehydrogenase (*GAPDH*), coproporphyrinogen oxidase (*CPOX*), protoporphyrinogen oxidase (*PPOX*), ferrochelatase (*FECH*), heme oxygenase 1 (*HO-1*), adenosine triphosphate (ATP)-binding cassette transporter G2 (*ABCG2*), ATP-binding cassette transporter B6 (*ABCB6*), hypoxia-inducible factor-1 alpha subunit (*HIF-1α*), lactate dehydrogenase A (*LDHA*), lactate dehydrogenase B (*LDHB*), pyruvate dehydrogenase kinase 1 (*PDK1*), vascular endothelial growth factor A (*VEGF*).

Figures

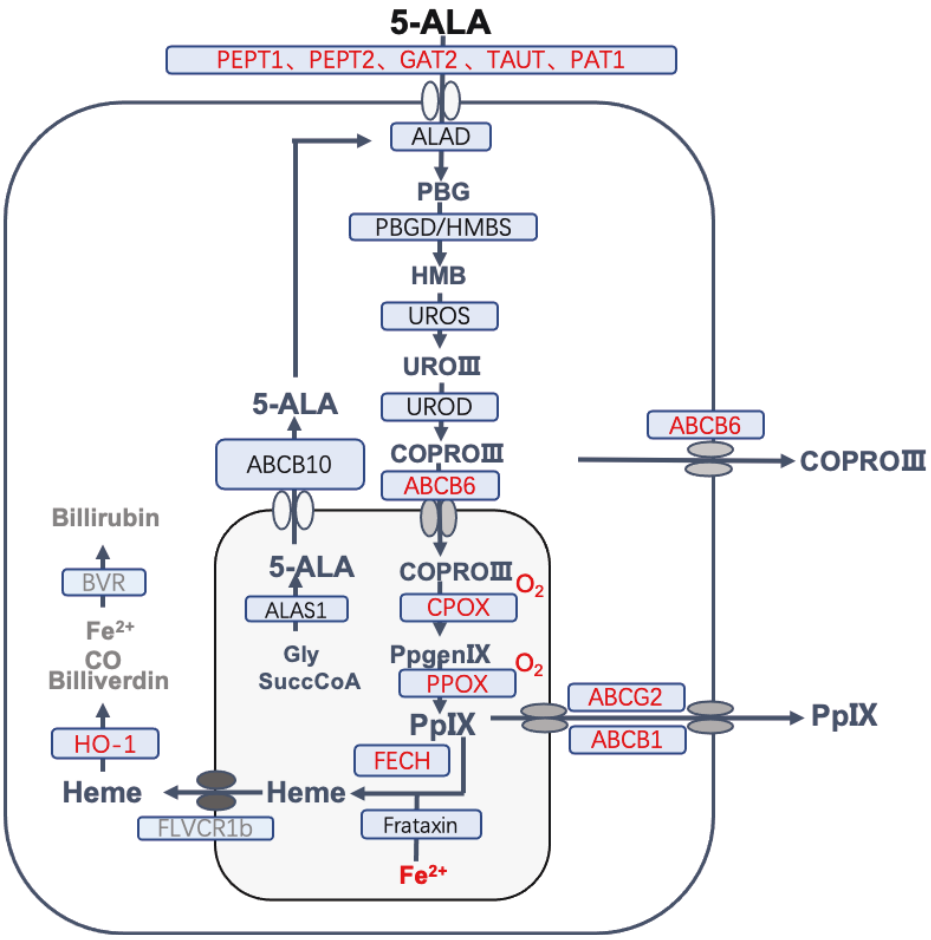

Figure 1. Mechanism of cellular uptake of 5-aminolevulinic acid (5-ALA) for protoporphyrin IX (PpIX) biosynthesis.

Peptide transporter 1 (*PEPT1*), peptide transporter 2 (*PEPT2*), gamma amino butyric acid transporter 2 (*GAT2*), taurine transporter (*TAUT*), H+/amino acid transporter 1 (*PAT1*), 5'-aminolevulinate synthase 1 (*ALAS1*), aminolevulinate dehydratase (*ALAD*), hydroxymethylbilane synthase (*HMBS*), uroporphyrinogen III synthase (*UROS*), uroporphyrinogen III decarboxylase (*UROD*), glyceraldehyde-3-phosphate dehydrogenase (*GAPDH*), coproporphyrinogen oxidase (*CPOX*), protoporphyrinogen oxidase (*PPOX*), ferrochelatase (*FECH*), heme oxygenase 1 (*HO-1*), adenosine triphosphate (ATP)-binding cassette transporter G2 (*ABCG2*), ATP-binding cassette transporter B6 (*ABCB6*), hypoxia-inducible factor-1 alpha subunit (*HIF-1α*), lactate dehydrogenase A (*LDHA*), lactate dehydrogenase B (*LDHB*), pyruvate dehydrogenase kinase 1 (*PDK1*), vascular endothelial growth factor A (*VEGF*).

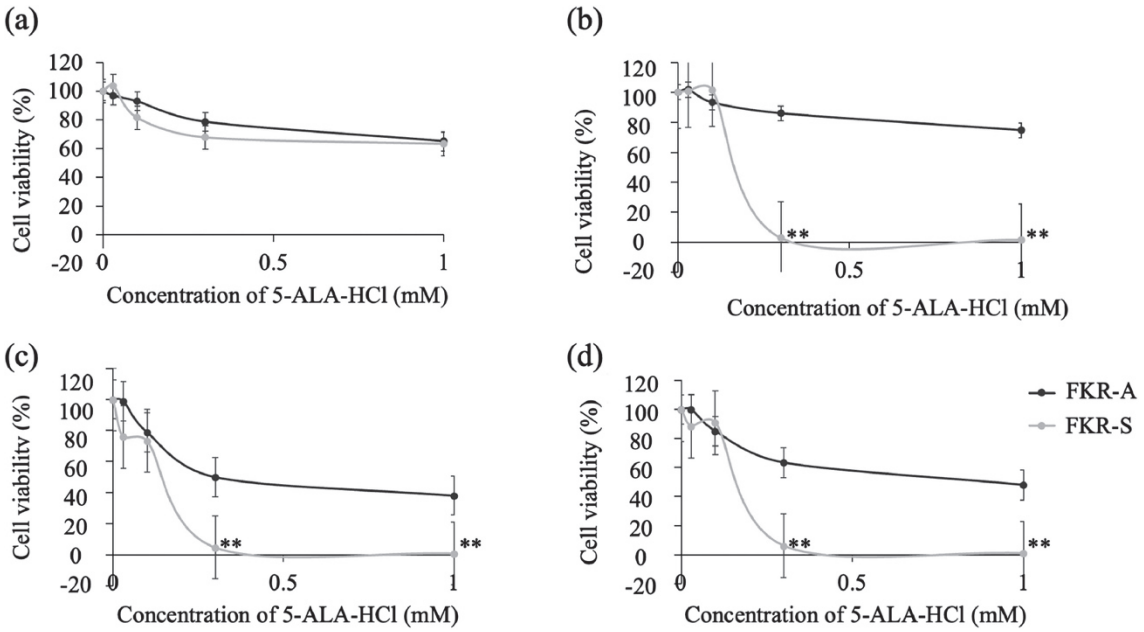

Figure 2. Cell viability.

(a) Light fluence rate: 0 mW/cm^2, light fluence: 0 J/cm^2, (b) Light fluence rate: 20 mW/cm^2, light fluence 5 J/cm^2, (c) Light fluence rate: 20 mW/cm^2, light fluence 10 J/cm^2, (d) Light fluence rate: 20 mW/cm^2, light fluence: 20 J/cm^2.

To determine the cytotoxic effect of photodynamic therapy with 5-aminolevulinic acid hydrochloride (5-ALA-HCl) on FKR-A and FKR-S cells, cells are treated with 4 different concentrations (0.03, 0.1, 0.3, and 1 mM) of 5-ALA-HCl and then irradiated with 5, 10, and 20 J/cm^2 (20 mW/cm^2). Results are presented as mean ± standard deviation (n = 3~6). **Significantly different at p<0.01.

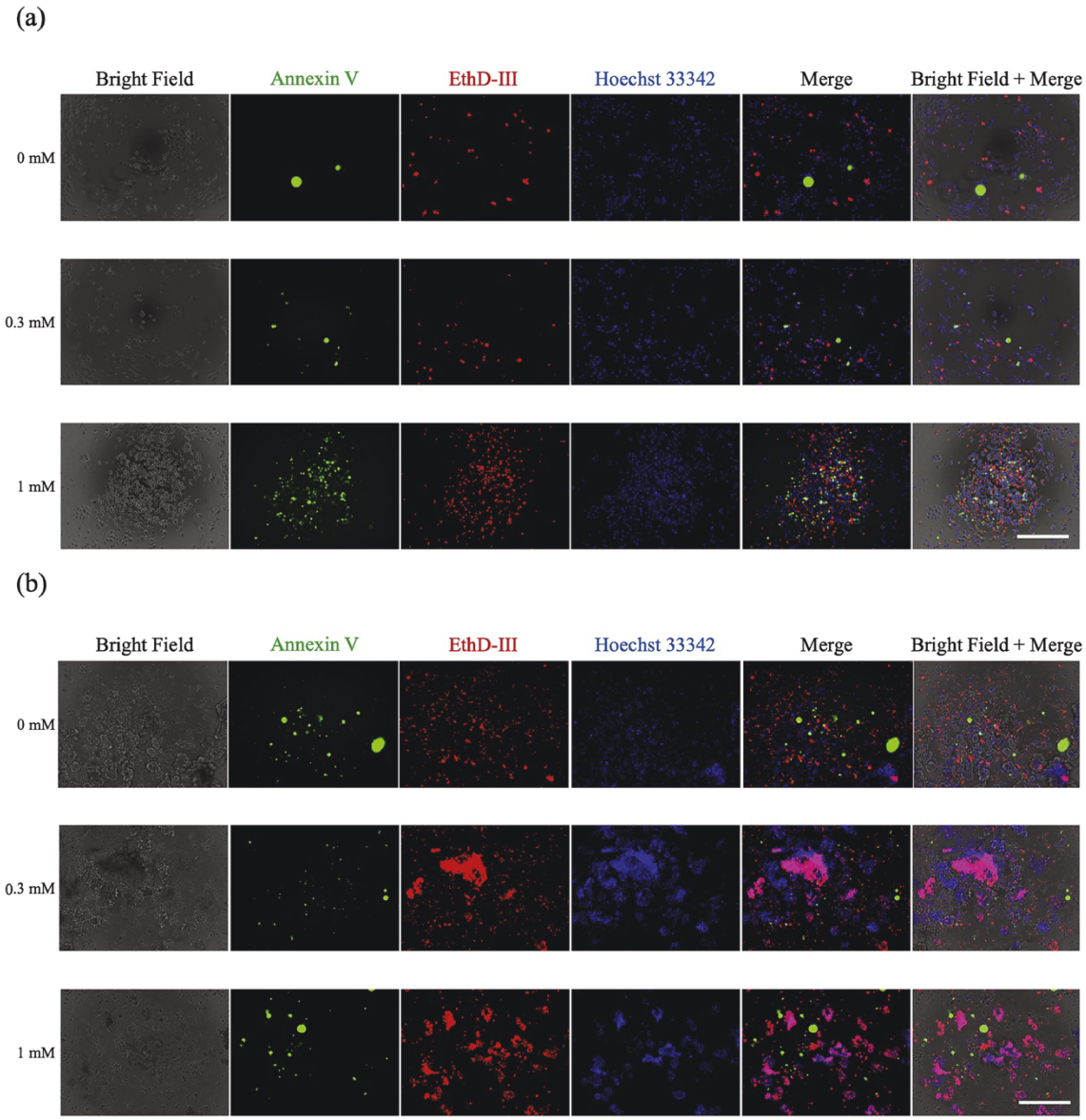

Figure 3. Evaluation of cell death. (a) FKR-A cells; (b) FKR-S cells.

Annexin V-stained apoptotic cells appear green. Ethidium Homodimer III-stained necrotic cells appear red, and Hoechst 33342-stained live cells have bright blue nuclei. Scale bar = 500 μm. Images are acquired 24 h after photodynamic therapy.

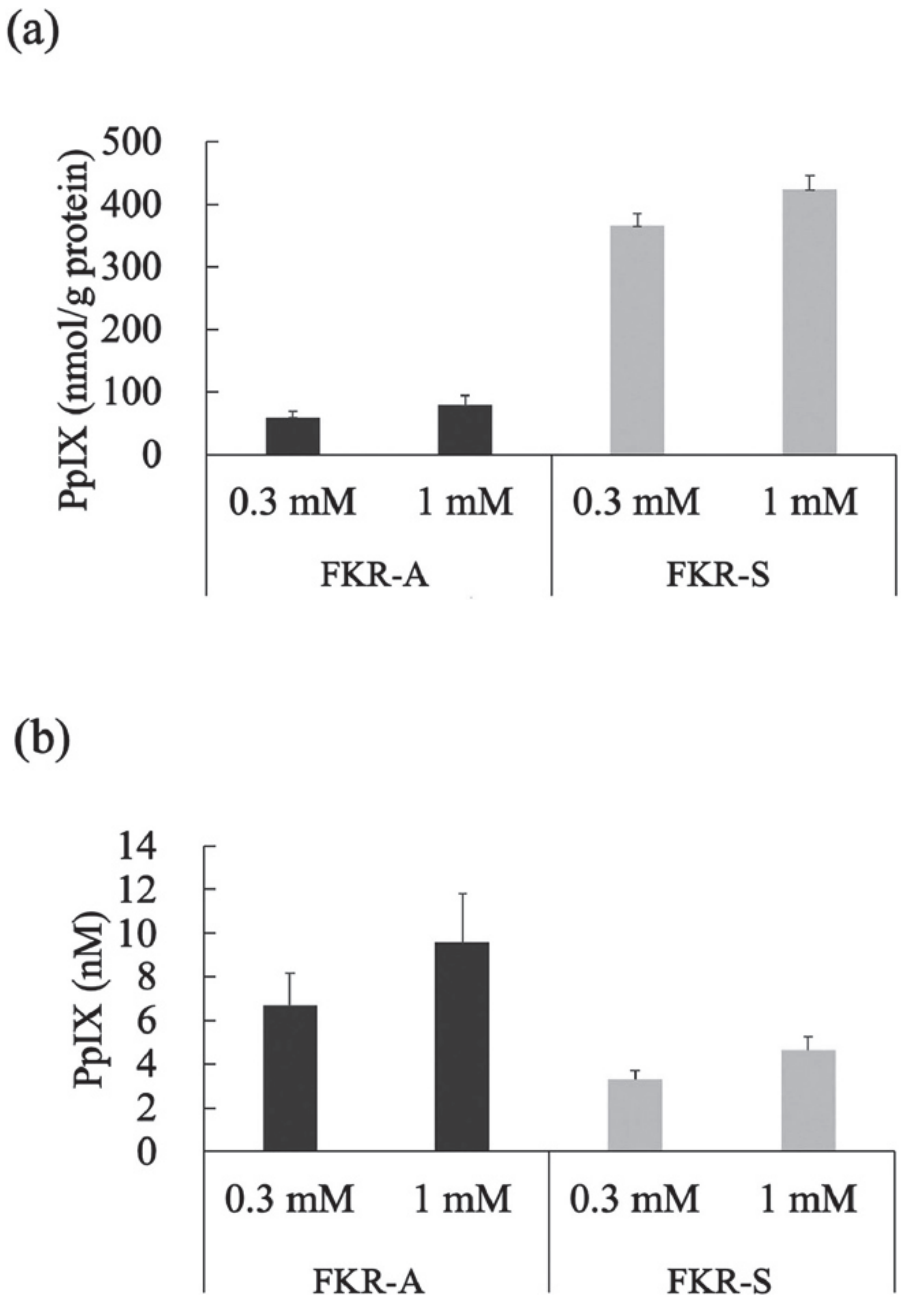

Figure 4. Intracellular protoporphyrin IX concentration in FKR-A and FKR-S Cells.

(a) Intracellular protoporphyrin IX (PpIX) concentration, (b) Extracellular PpIX concentration.

Results are presented as mean ± standard deviation (n = 3).

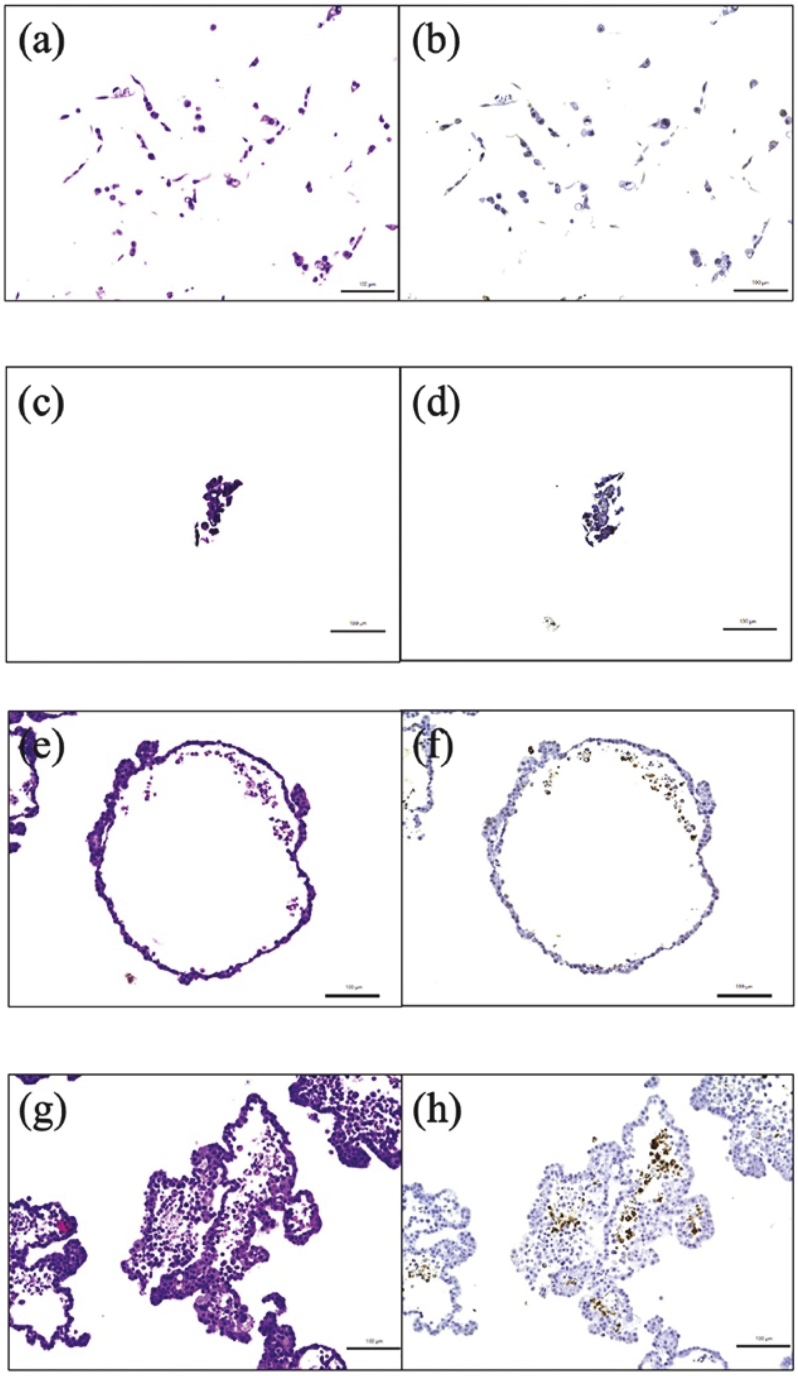

Figure 5. Histological evaluation.

All experimental groups use 0.3 mM 5-aminolevulinic acid hydrochloride (5-ALA-HCl), and cells are irradiated with an LED light (630 nm, 20 mW/cm^2, 10 J/cm^2).
(a-d) FKR-A cells; (e-h) FKR-S cells, (a,e) Hematoxylin and eosin (H&E) staining of the control group, (b,f) Terminal deoxynucleotidyl transferase dUTP nick end labeling (TUNEL) staining of the control group, (c,g) H&E staining after 5-ALA-photodynamic therapy (PDT), (d,h) TUNEL staining after 5-ALA-PDT.
Images after 24 h of PDT. Scale bars = 100 μm.

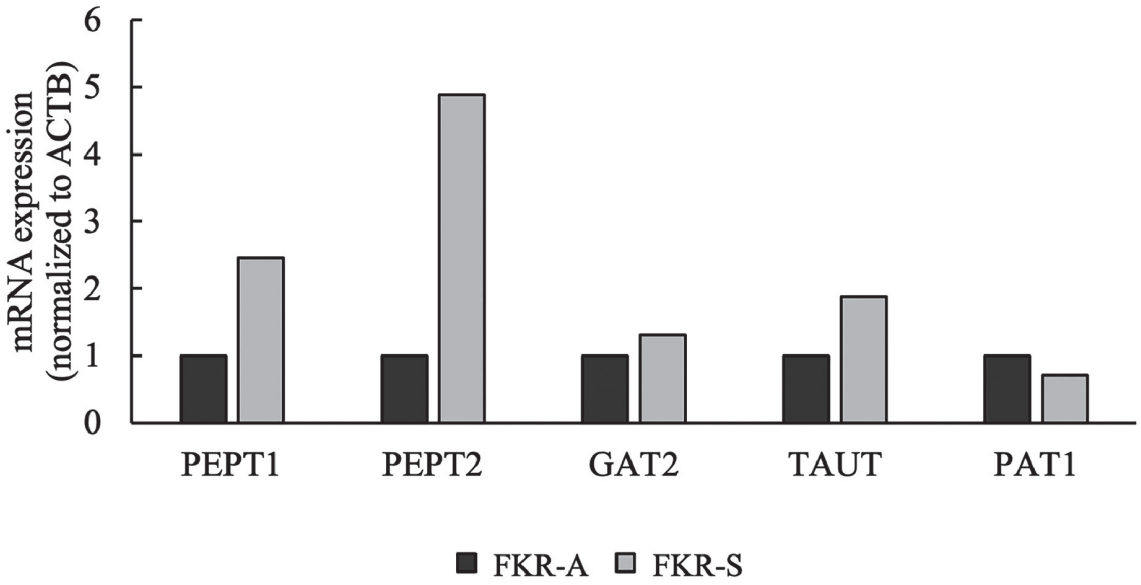

Figure 6. 5-aminolevulinic acid uptake transporter gene.

Peptide transporter 1 (*PEPT1*), peptide transporter 2 (*PEPT2*), GABA transporter 2 (*GAT2*), taurine transporter (*TAUT*), and H+/amino acid transporter 1 (*PAT1*). Results are presented as mean ± standard deviation (triplicates).

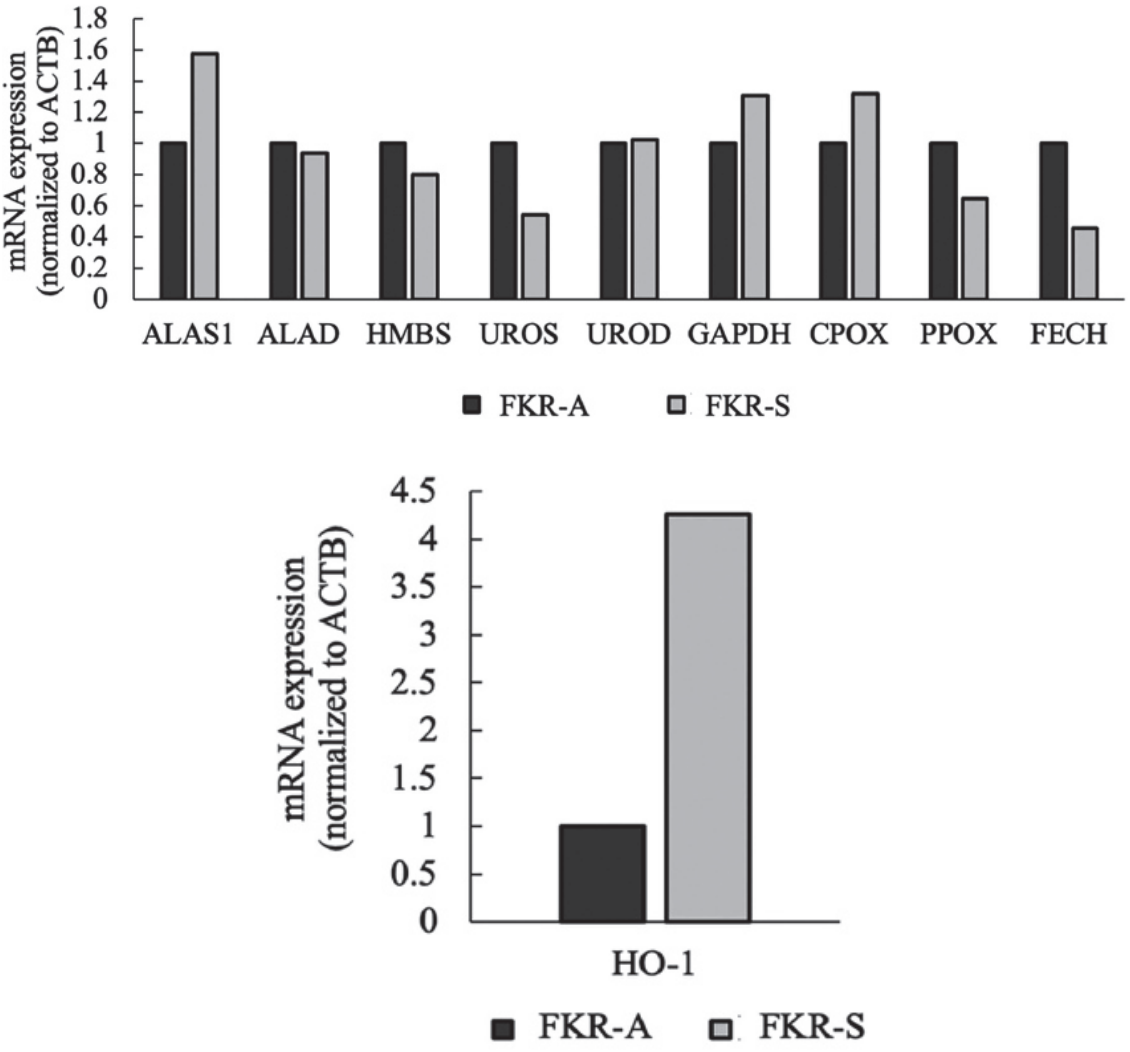

Figure 7. Genes related to heme synthesis (heme synthase).

5'-aminolevulinate synthase 1 (*ALAS1*), aminolevulinate dehydratase (*ALAD*), hydroxymethylbilane synthase (*HMBS*), uroporphyrinogen III synthase (*UROS*), uroporphyrinogen III decarboxylase (*UROD*), coproporphyrinogen oxidase (*CPOX*), protoporphyrinogen oxidase (*PPOX*), ferrochelatase (*FECH*), and Heme oxygenase 1 (*HO-1*). Results are presented as mean ± standard deviation (triplicates).

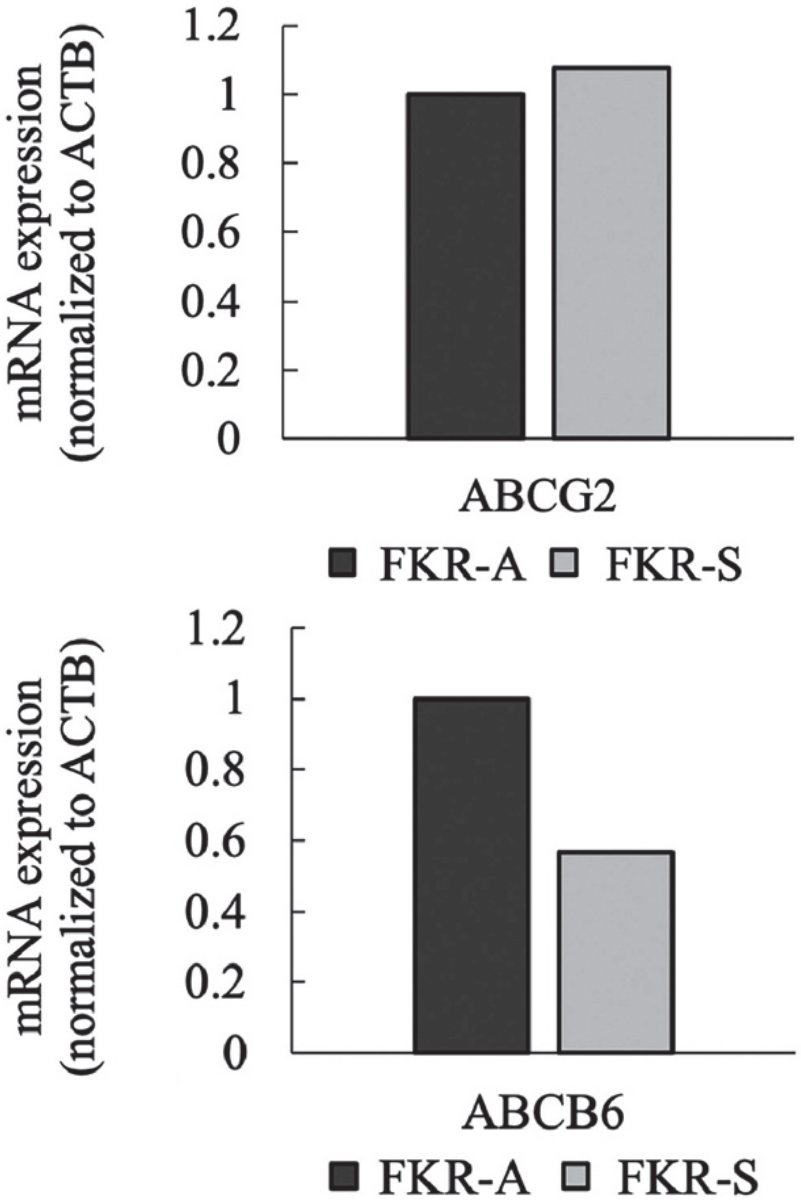

Figure 8. **Porphyrin excretion transporter gene.**

ATP-binding cassette transporters G2 (*ABCG2*) and B6 (*ABCB6*). Results are presented as mean ± standard deviation (triplicates).

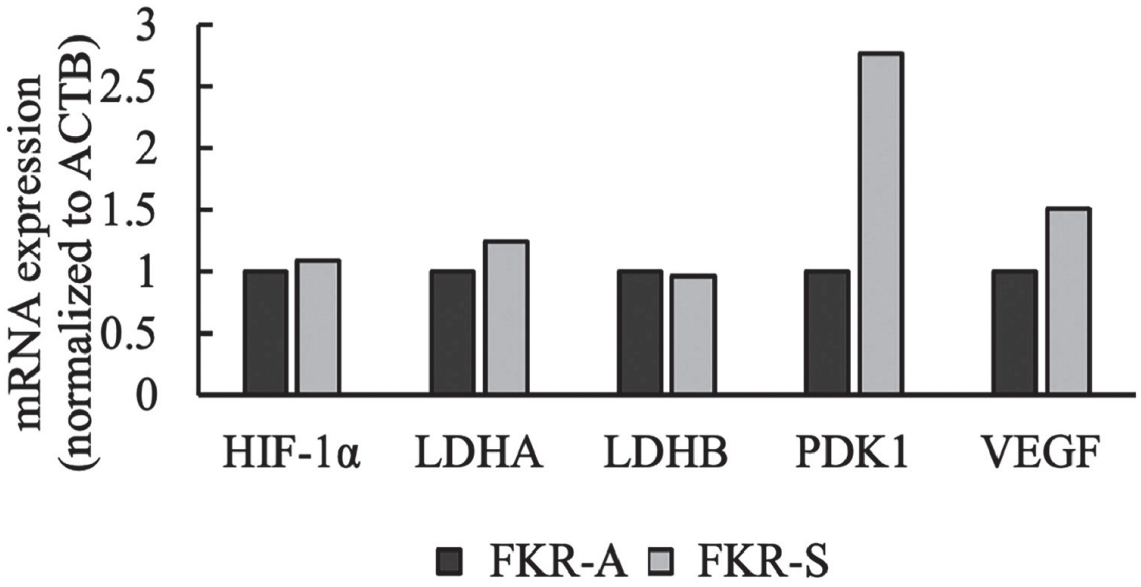

Figure 9. **Hypoxia-related genes.**

Hypoxia-inducible factor 1 alpha subunit (*HIF-1α*), lactate dehydrogenase A (*LDHA*), lactate dehydrogenase B (*LDHB*), pyruvate dehydrogenase kinase 1 (*PDK1*), and vascular endothelial growth factor A (*VEGF*). Results are presented as mean ± standard deviation (triplicates).

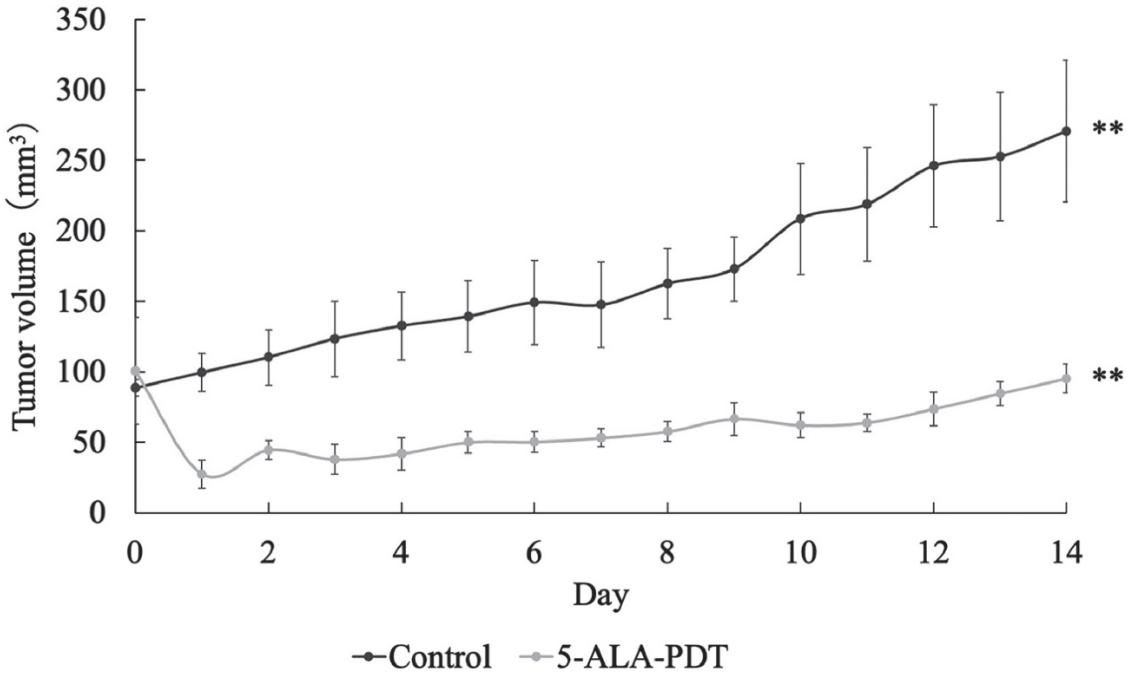

Figure 10. Changes in tumor volume.

Mice were intraperitoneally injected with 250 mg/kg 5-aminolevulinic acid hydrochloride (5-ALA-HCl), and 4 h later, photodynamic therapy (PDT) were performed using a 636 nm laser (250 mW/cm^2, 150 J/cm^2). Data are presented as mean ± SD (n = 4). Data represent the mean relative tumor volume normalized to that on the day of therapy initiation (day 0). The bars indicate standard errors. **Significantly different at $p<0.01$.

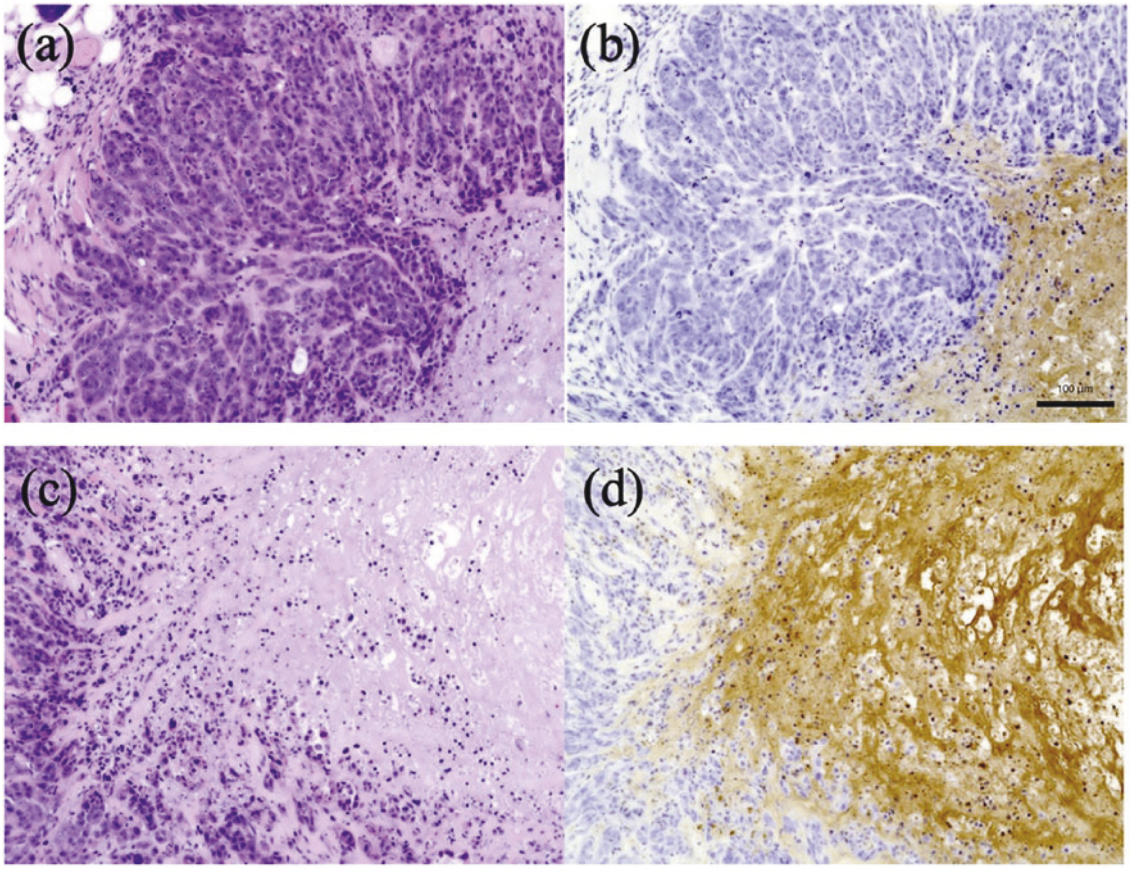

Figure 11. Histopathological section after 24 h of photodynamic therapy (PDT) with 5-aminolevulinic acid hydrochloride (5-ALA-HCl).

(a) Hematoxylin and eosin (H&E) staining of the control group, (b) terminal deoxynucleotidyltransferase-mediated dUTP nick end labeling (TUNEL) staining of the control group, (c) H&E staining after 5-ALA-PDT, (d) TUNEL staining after 5-ALA-PDT. Scale bars = 100 µm.

CHAPTER 3

General conclusion

Mammary tumors are one of the most common tumors in felines. Although primary FMTs can be surgically resected, the prognosis is often poor because of the development of pulmonary metastases or metastasis to body surface lymph nodes. In addition, new palliative treatments are needed for recurrent cases or for cases that do not tolerate surgery. PDT, which is low invasive, selectively causes apoptosis and necrosis of tumors, and can be used with other therapies, is one of the novel therapies for treating tumors. However, PDT has done little research related to the treatment of FMTs. This study aimed to evaluate the efficacy of 5-ALA-PDT against FMTs and assess the factors affecting this therapy by alterations in cell morphology.

Based on *in vitro* studies, the author evaluated the cell viability of FMTs FKR-S and FKR-A under 5-ALA-PDT. A cytotoxic effect of 5-ALA-PDT on FKR-S and FKR-A was demonstrated, and a significant difference in cytotoxicity was produced between the two (stronger toxicity on 3D-cultured FKR-S than on 2D-cultured FKR-A). The author concluded that 5-ALA-PDT reduced cell viability in a PS-dose-dependent manner. The higher the 5-ALA concentration and light intensity, the lower the cell viability.

At the same dose of 5-ALA, the intracellular PpIX concentration in FKR-A cells was approximately 20% that in FKR-S. Therefore, the authors investigated the expression levels of various genes that may affect ALA-mediated PpIX accumulation. These results suggest that compared to FKR-S, the low expression of *PEPT1*, *PEPT2*, and *ALAS1* in FKR-A cells, in synergy with the high expression levels of *ABCB6* and *FECH*, among others, resulted in lower intracellular accumulation of PpIX. PDT was less effective than in FKR-S cells. These findings suggest that the uptake mechanisms of 2D cells and 3D spheroids may differ, even for homologous tumor cells.

In this study, cell death assessment showed that 5-ALA-PDT induced apoptosis and

necrosis.

In addition, the *in vivo* inhibitory effect of 5-ALA-PDT on FKR-S tumor cells was evaluated. Mean tumor volume was reduced after a single 24-hour treatment with 5-ALA-PDT. Histological examination after 14 days also revealed many necrotic cells after PDT, suggesting that a single 5-ALA-PDT could have an inhibitory effect on the persistence of mammary tumor development in NOD/ShiJic-scidJcl mice.

A notable limitation of the present study is that a subcutaneous xenograft mouse model was used. This does not allow for a completely accurate assessment of the effect of 5-ALA-PDT when FKR cells are grown in FMTs. The development of an orthotopic xenograft mouse model should be considered in future studies. We also investigated gene expression *in vivo*; however, because of the invasion of mouse cells, we were unable to obtain accurate results. Therefore, we were unable to confirm whether gene expression *in vivo* is the same as gene expression *in vitro*.

In conclusion, the author believes that 5-ALA-PDT is effective for FMT. 5-ALA-PDT exerts cytotoxic effects in a PS-dose-dependent manner. Even in homologous tumor cells, differences in cell morphology and mRNA expression levels can lead to different sensitivities to PDT. 5-ALA-PDT can inhibit in-vivo FMT growth. The author believes that establishing an *in-vitro* tumor model closer to a living organism for use in 5-ALA-PDT-related research will yield more accurate and effective results.

References

1. S. W. Mills, K. M. Musil, J. L. Davies, S. Hendrick, C. Duncan, M. L. Jackson, B. Kidney, H. Philibert, B. K. Wobeser, E. Simko. Prognostic value of histologic grading for feline mammary carcinoma: a retrospective survival analysis, Veterinary Pathology. 52, 2 (2015): 238–249.
2. K. Hughes, J. Dobson. Prognostic histopathological and molecular markers in feline mammary neoplasia, Veterinary journal. 194, 1 (2012): 19–26.
3. M. Soares, J. Correia, C. Nascimento, F. Ferreira. Anaplastic mammary carcinoma in cat, Veterinary Sciences. 8 (2021).
4. F. V. Amorim, H. Souza, A. M. Ferreira, A. Fonseca. Clinical, cytological and histopathological evaluation of mammary masses in cats from Rio de Janeiro, Brazil, Journal of Feline Medicine and Surgery. 8 (2006): 379–388.
5. M. Soares, Jorge Correia, M. Peleteiro, F. Ferreira. St Gallen molecular subtypes in feline mammary carcinoma and paired metastases—disease progression and clinical implications from a 3-year follow-up study, Tumor Biology. 37 (2016): 4053–4064.
6. F. Seixas, C. Palmeira, M. Pires, M. Bento, Carlos A Lopes. Grade is an independent prognostic factor for feline mammary carcinomas: a clinicopathological and survival analysis, Veterinary journal. 187, 1 (2011): 65–71.
7. B. Hassan, S. M. Elshafae, W. Supsavhad, J. K. Simmons, W. P. Dirksen, S. Sokkar, T. J. Rosol. Feline mammary cancer, Veterinary Pathology. 54 (2017): 32–43.
8. M. Soares, S. Madeira, J. Correia, M. Peleteiro, F. Cardoso, F. Ferreira. Molecular based subtyping of feline mammary carcinomas and clinicopathological characterization, Breast. 27 (2016): 44–51.
9. P. P. Price, A. Stell, D. O'Neill, D. Church, D. Brodbelt. Epidemiology and risk factors

for mammary tumours in female cats, The Journal of Small Animal Practice. 64, 5 (2023): 313–320.

10. B. Overley, F. S. Shofer, M. H. Goldschmidt, D. Sherer, K. U. Sorenmo. Association between ovarihysterectomy and feline mammary carcinoma, Journal of Veterinary Internal Medicine. 19, 4 (2005): 560–563.
11. J. Morris. Mammary tumours in the cat: size matters, so early intervention saves lives, Journal of Feline Medicine and Surgery. 15, 5 (2013): 391–400.
12. F. Giménez, S. Hecht, L. E. Craig, A. M. Legendre. Early detection, aggressive therapy: optimizing the management of feline mammary masses, Journal of Feline Medicine and Surgery. 12, 3 (2010): 214–224.
13. C. A. Novosad. Principles of treatment for mammary gland tumors, Clinical Techniques in Small Animal Practice. 18, 2 (2003): 107–109.
14. F. Gemignani, P. Mayhew, M. Giuffrida, J. Palaigos, J. Runge, D. Holt, N. Robertson, B. Séguin, M. Walker, A. Singh, J. Liptak, G. Romanelli, M. Martano, S. Boston, C. Lux, R. Busetto, W. Culp, K. Skorupski, J. Burton. Association of surgical approach with complication rate, progression-free survival time, and disease-specific survival time in cats with mammary adenocarcinoma: 107 cases (1991-2014), Journal of the American Veterinary Medical Association. 252, 11 (2018): 1393–1402.
15. M. Castagnaro, C. Casalone, E. Bozzetta, R. De Maria, B. Biolatti, M. Caramelli. Tumour grading and the one-year post-surgical prognosis in feline mammary carcinomas, Journal of Comparative Pathology. 119, 3 (1998): 263–275.
16. S. Cunha, K. B. Corgozinho, H. Souza, K. Silva, A. M. Ferreira. Adjuvant chemotherapy with mitoxantrone for cats with mammary carcinomas treated with radical mastectomy, Journal of Feline Medicine and Surgery. 17 (2015): 1000–1004.

17. C. B. de Campos, F. C. Nunes, G. Lavalle, G. Cassali. Use of surgery and carboplatin in feline malignant mammary gland neoplasms with advanced clinical staging, In vivo. 28, 5 (2014): 863–866.
18. S. Pushpan, S. Venkatraman, V. Anand, J. Sankar, D. Parmeswaran, S. Ganesan, T. K. Chandrashekar. Porphyrins in photodynamic therapy—a search for ideal photosensitizers, Current Medicinal Chemistry, Anti-Cancer Agents. 2, 2 (2002): 187–207.
19. M. Daniell, J. Hill. A history of photodynamic therapy, The Australian and New Zealand Journal of Surgery. 61, 5 (1991): 340–348.
20. R. Ackroyd, C. Kelty, N. Brown, M. Reed. The history of photodetection and photodynamic therapy, Photochemistry and Photobiology. 74, 5 (2001): 656–669.
21. D. Mitton, R. Ackroyd. A brief overview of photodynamic therapy in Europe, Photodiagnosis and Photodynamic Therapy. 5, 2 (2008): 103–111.
22. J. Correia, J. A. Rodrigues, S. Pimenta, T. Dong, Z. Yang. Photodynamic therapy review: principles, photosensitizers, applications, and future directions, Pharmaceutics. 13, 9 (2021): 1332.
23. D. Straten, V. Mashayekhi, H. S. Bruijn, S. Oliveira, D. J. Robinson. Oncologic photodynamic therapy: basic principles, current clinical status and future directions, Cancers (Basel). 9, 2 (2017): 19.
24. D. E. Dolmans, D. Fukumura, R. Jain. Photodynamic therapy for cancer, Nature Reviews Cancer. 3 (2003): 380–387.
25. R. Ramponi, C. Sacchi, R. Cubeddu. Present status of research on hematoporphyrin derivatives and their photophysical properties, Laser Applications in Medicine and Biology. (1991): 49–84.

26. R. L. Lipson, E. J. Baldes, A. M. Olsen. The use of a derivative of hematoporhyrin in tumor detection, Journal of the National Cancer Institute. 26 (1961): 1–11.
27. I. Diamond, S. G. Granelli, A. F. Mcdonagh, S. Nielsen, C. B. Wilson, R. Jaenicke. Photodynamic therapy of malignant tumours, Lancet. 2, 7788 (1972): 1175–1177.
28. T. J. Dougherty, G. B. Grindey, R. Fiel, K. R. Weishaupt, D. G. Boyle. Photoradiation therapy. II. cure of animal tumors with hematoporphyrin and light, Journal of the National Cancer Institute. 55, 1 (1975): 115–121.
29. J. J. Schuitmaker, P. Baas, H. L. Leengoed, F. W. Meulen, W. M. Star, N. Zandwijk. Photodynamic therapy: a promising new modality for the treatment of cancer, Journal of Photochemistry and Photobiology, B, Biology. 34, 1 (1996): 3–12.
30. Y. Hayata, H. Kato, C. Konaka, J. Ono, N. Takizawa. Hematoporphyrin derivative and laser photoradiation in the treatment of lung cancer, Chest. 81, 3 (1982): 269–277.
31. T. J. Dougherty, J. E. Kaufman, A. Goldfarb, K. R. Weishaupt, D. Boyle, A. Mittleman. Photoradiation therapy for the treatment of malignant tumors, Cancer Research. 38, 8 (1978): 2628–2635.
32. P. Agostinis, K. Berg, K. Cengel, T. Foster, A. Girotti, S. Gollnick, S. Hahn, Michael R Hamblin, A. Juzeniene, D. Kessel, M. Korbelik, J. Moan, P. Mróz, D. Nowis, J. Piette, B. Wilson, J. Gołąb. Photodynamic therapy of cancer: an update, CA: A Cancer Journal for Clinicians. 61, 4 (2011): 250–281
33. H. Gong, Y. Chao, J. Xiang, X. Han, G. Song, L. Feng, J. Liu, G. Yang, Q. Chen, Z. Liu. Hyaluronidase to enhance nanoparticle-based photodynamic tumor therapy, Nano Letters. 16, 4 (2016): 2512–2521.
34. R. Vankayala, K. Hwang. Near-infrared-light-activatable nanomaterial-mediated phototheranostic nanomedicines: an emerging paradigm for cancer

treatment, Advanced Materials. 30, 23 (2018): e1706320.

35. S. Galadari, A. Rahman, S. Pallichankandy, F. Thayyullathil. Reactive oxygen species and cancer paradox: to promote or to suppress? Free Radical Biology and Medicine. 104 (2017): 144–164.
36. P. Jia, C. Dai, P. Cao, D. Sun, R. Ouyang, Y. Miao. The role of reactive oxygen species in tumor treatment, RSC Advances. 10,13 (2020): 7740–7750.
37. J. Moan, K. Berg. The photodegradation of porphyrins in cells can be used to estimate the lifetime of singlet oxygen, Photochemistry and Photobiology. 53,4 (1991): 549–553.
38. T. J. Dougherty, C. J. Gomer, B. W. Henderson, G. Jori, D. Kessel, M. Korbelik, J. Moan, Q. Peng. Photodynamic therapy, Journal of National Cancer Institute. 90, 12 (1998): 889–905.
39. A. P. Castano, P. Mroz, M. R. Hamblin. Photodynamic therapy and anti-tumour immunity, Nature Reviews Cancer. 6, 7 (2006): 535–545.
40. N. L. Oleinick, R. L. Morris, I. Belichenko. The role of apoptosis in response to photodynamic therapy: what, where, why, and how, Photochemical & Photobiological Sciences. 1, 1 (2002): 1–21.
41. D. Kessel, R. Luguya, M. G. H. Vicente. Localization and photodynamic efficacy of two cationic porphyrins varying in charge distributions, Photochem Photobiol. 78, 5 (2003): 431–435.
42. Y. Luo, D. Kessel. Initiation of apoptosis versus necrosis by photodynamic therapy with chloroaluminum phthalocyanine, Photochem Photobiol. 66,4 (1997): 479–483.
43. G. Lavie, C. Kaplinsky, A. Toren, I. Aizman, D. Meruelo, Y. Mazur, M. Mandel. A photodynamic pathway to apoptosis and necrosis induced by dimethyl

tetrahydroxyhelianthrone and hypericin in leukaemic cells: possible relevance to photodynamic therapy, British Journal of Cancer. 79 (1999): 423–432.

44. V. H. Fingar, T. J. Wieman, P. S. Haydon. The effects of thrombocytopenia on vessel stasis and macromolecular leakage after photodynamic therapy using photofrin, Photochemistry and Photobiology. 66, 4 (1997): 513–517.
45. V. H. Fingar, P. K. Kik, P. S. Haydon, P. B. Cerrito, M. Tseng, E. Abang, T. J. Wieman. Analysis of acute vascular damage after photodynamic therapy using benzoporphyrin derivative (BPD), British Journal of Cancer. 79, 11–12 (1999): 1702–1708.
46. D. Dolmans, A. Kadambi, J. S. Hill, C. A. Waters, B. C. Robinson, J. P. Walker, D. Fukumura, R. K. Jain. Vascular accumulation of a novel photosensitizer, MV6401, causes selective thrombosis in tumor vessels after photodynamic therapy, Cancer Research. 62, 7 (2002): 2151–2156.
47. S. O. Gollnick, X. Liu, B. Owczarczak, D. A. Musser, B. W. Henderson. Altered expression of interleukin 6 and interleukin 10 as a result of photodynamic therapy *in vivo*, Cancer Research. 57, 18 (1997): 3904–3909.
48. W. J. Vree, M. C. Essers, H. S. D. Bruijn, W. M. Star, J. F. Koster, W. Sluiter. Evidence for an important role of neutrophils in the efficacy of photodynamic therapy *in vivo*, Cancer Research. 56, 13 (1996): 2908–2911.
49. M. Korbelik, G. Krosl, J. Krosl, G. J. Dougherty. The role of host lymphoid populations in the response of mouse EMT6 tumor to photodynamic therapy, Cancer Research. 56, 24 (1996): 5647–5652.
50. I. O. L. Bacellar, T. M. Tsubone, C. Pavani, M. Baptista. Photodynamic efficiency: from molecular photochemistry to cell death, International Journal of Molecular Sciences. 16, 9 (2015): 20523–20559.

51. F. H. Igney, P. H. Krammer. Death and anti-death: Tumour resistance to apoptosis, Nature Reviews Cancer. 2, 4 (2002): 277–288.

52. P. Mroz, A. Yaroslavsky, G. B. Kharkwal, Michael R Hamblin. Cell death pathways in photodynamic therapy of cancer, Cancers. 3 (2011): 2516–2539.

53. S. Nagata, A. Obana, Y. Gohto, S. Nakajima. Necrotic and apoptotic cell death of human malignant melanoma cells following photodynamic therapy using an amphiphilic photosensitizer, ATX-S10(Na), Lasers in Surgery and Medicine. 33, 1 (2003): 64–70.

54. V. Inguscio, E. Panzarini, L. Dini. Autophagy contributes to the death/survival balance in cancer photodynamic therapy, Cells. 1, 3 (2012): 464–491.

55. D. Kessel, M.G. H. Vicente, J. J. Reiners Jr. Initiation of apoptosis and autophagy by photodynamic therapy, Autophagy. 2, 4 (2006): 289–290.

56. E. Buytaert, G. Callewaert, N. Hendrickx, L. Scorrano, D. Hartmann, L. Missiaen, J. R. Vandenheede, I. Heirman, J. Grooten, P. Agostinis. Role of endoplasmic reticulum depletion and multidomain proapoptotic bax and bak proteins in shaping cell death after hypericin-mediated photodynamic therapy, FASEB Journal: Official Publication of the Federation of American Societies for Experimental Biology. 20, 6 (2006): 756–758.

57. L. Xue, S. Chiu, K. Azizuddin, S. Joseph, N. L. Oleinick. The death of human cancer cells following photodynamic therapy: apoptosis competence is necessary for Bcl-2 protection but not for induction of autophagy, Photochemistry and Photobiology. 83, 5 (2007): 1016–1023.

58. D. Kessel, N. L. Oleinick. Initiation of autophagy by photodynamic therapy, Methods in Enzymology. 453 (2009): 1–16.

59. J. C. Kennedy, R. H. Pottier. Endogenous protoporphyrin IX, a clinically useful photosensitizer for photodynamic therapy, Journal of Photochemistry and Photobiology B, Biology. 14, 4 (1992): 275–292.

60. M. Sachar, K. E. Anderson, X. Ma. Protoporphyrin IX: the good, the bad, and the ugly, The Journal of Pharmacology and Experimental Therapeutics. 356, 2 (2016): 267–275.

61. G. C. Ferreira, R. Franco, S. G. Lloyd, I. Moura, J. J. Moura, B. H. Huynh. Structure and function of ferrochelatase, Journal of Bioenergetics and Biomembranes. 27, 2 (1995): 221–229.

62. S. Kaneko, S. Kaneko. Fluorescence-guided resection of malignant glioma with 5-ALA, International Journal of Biomedical Imaging. 2016 (2016): 6135293.

63. N. Mehraban, H. S. Freeman. Developments in PDT sensitizers for increased selectivity and singlet oxygen production, Materials. 8, 7 (2015): 4421–4456.

64. S. L. Ratcliffe, E. K. Matthews. Modification of the photodynamic action of delta-aminolaevulinic acid (ALA) on rat pancreatoma cells by mitochondrial benzodiazepine receptor ligands, British Journal of Cancer. 71, 2 (1995): 300–305.

65. M. Ishizuka, F. Abe, Y. Sano, K. Takahashi, K. Inoue, M. Nakajima, T. Kohda, N. Komatsu, S. Ogura, T. Tanaka. Novel development of 5-aminolevurinic acid (ALA) in cancer diagnoses and therapy, International Immunopharmacology. 11, 3 (2011): 358–365.

66. S. Taketani. Aquisition, mobilization and utilization of cellular iron and heme: endless findings and growing evidence of tight regulation, The Tohoku Journal of Experimental Medicine. 205, 4 (2005): 297–318.

67. A. S. Tsiftsoglou, A. I. Tsamadou, L. C. Papadopoulou. Heme as key regulator of

major mammalian cellular functions: molecular, cellular, and pharmacological aspects, Pharmacology & therapeutics. 111, 2 (2006): 327–345.

68. S. I. Woodard, H. A. Dailey. Multiple regulatory steps in erythroid heme biosynthesis, Archives of Biochemistry and Biophysics. 384, 2 (2000): 375–378.
69. B. E. Dwyer, M. A. Smith, S. L. Richardson, G. Perry, X. Zhu. Down-regulation of aminolevulinate synthase, the rate-limiting enzyme for heme biosynthesis in Alzheimer's disease, Neuroscience Letters. 460, 2 (2009): 180–184.
70. P. C. Krishnamurthy, G. Du, Y. Fukuda, D. Sun, J. Sampath, K. E. Mercer, J. Wang, B. S. Pineda, K. G. Murti, J. D. Schuetz. Identification of a mammalian mitochondrial porphyrin transporter, Nature. 443, 7111 (2006): 586–589.
71. D.L. Ulrich, J. Lynch, Y. Wang, Y. Fukuda, D. Nachagari, G. Du, D. Sun, Y. Fan, L. Tsurkan, P. M. Potter, J. E. Rehg, J. D. Schuetz. ATP-dependent mitochondrial porphyrin importer ABCB6 protects against phenylhydrazine toxicity, The Journal of Biological Chemistry. 287, 16 (2012): 12679–12690.
72. M. M. Gottesman, T. Fojo, S. E. Bates. Multidrug resistance in cancer: role of ATP-dependent transporters, Nature Reviews Cancer. 2, 1 (2002): 48–58.
73. M. Solazzo, O. Fantappiè, M. D'Amico, C. Sassoli, A. Tani, G. Cipriani, C. Bogani, L. Formigli, R. Mazzanti. Mitochondrial expression and functional activity of breast cancer resistance protein in different multiple drug-resistant cell lines, Cancer Research. 69, 18 (2009): 7235–7242.
74. P. Wang, M. Sachar, J. Lu, A. I. Shehu, J. Zhu, J. Chen, K. Liu, K. E. Anderson, W. Xie, F. J. Gonzalez, C. D. Klaassen, X. Ma. The essential role of the transporter ABCG2 in the pathophysiology of erythropoietic protoporphyria, Science Advances. 5, 9 (2019): eaaw6127.

75. S. Zhou, Y. Zong, P. A. Ney, G. Nair, C. F. Stewart, B. P. Sorrentino. Increased expression of the Abcg2 transporter during erythroid maturation plays a role in decreasing cellular protoporphyrin IX levels, Blood. 105, 6 (2005): 2571–2576.

76. G. W. Ibrahim, C. J. Watson. Enterohepatic circulation and conversion of protoporphyrin to bile pigment in man, Proceedings of the Society for Experimental Biology and Medicine. 127, 3 (1968): 890–895.

77. M. Thapar, H. L. Bonkovsky. The diagnosis and management of erythropoietic protoporphyria, Gastroenterology and Hepatology. 4, 8 (2008): 561–566.

78. Y. Lin, H. Chang, F. Chang, C. Shen, C. Liu, W. Mao, C. Lin, H. Lee, C. Shen. Protoporphyrin IX accumulation disrupts mitochondrial dynamics and function in ABCG2-deficient hepatocytes, FEBS Letters. 587, 19 (2013): 3202–3209.

79. V. S. Chelakkot, K. Liu, E. Yoshioka, S. Saha, D. Xu, M. Licursi, A. Dorward, Kensuke Hirasawa. MEK reduces cancer-specific PpIX accumulation through the RSK-ABCB1 and HIF-1α-FECH axes, Scientific Reports. 10, 1 (2020): 22124.

80. H. Liu, J. Lin, K. Roy. Effect of 3D scaffold and dynamic culture condition on the global gene expression profile of mouse embryonic stem cells, Biomaterials. 27, 36 (2006): 5978–5989.

81. V. M. Weaver, O. W. Petersen, F. Wang, C. A. Larabell, P. Briand, C. Damsky, M. J. Bissell. Reversion of the malignant phenotype of human breast cells in three-dimensional culture and *in vivo* by integrin blocking antibodies, The Journal of Cell Biology. 137, 1 (1997): 231–245.

82. S. Breslin, L. O'Driscoll. Three-dimensional cell culture: the missing link in drug discovery, Drug Discovery Today. 18, 5–6 (2013): 240–249.

83. M. C. Cox, L. M. Reese, L. R. Bickford, S. S. Verbridge. Toward the broad adoption

of 3D tumor models in the cancer drug pipeline, ACS Biomaterials Science & Engineering. 1, 10 (2015): 877–894.

84. O. Habanjar, M. D. Assaf, F. C. Chézet, L. Delort. 3D cell culture systems: tumor application, advantages, and disadvantages, International Journal of Molecular Sciences. 22, 22 (2021): 12200.

85. K. Stock, M. F. Estrada, S. Vidic, K. Gjerde, A. Rudisch, V. E. Santo, M. Barbier, S. Blom, S. C. Arundkar, I. Selvam, A. Osswald, Y. Stein, S. Gruenewald, C. Brito, W. V. Weerden, V. Rotter, E. Boghaert, M. Oren, W. Sommergruber, Y. Chong, R. Hoogt, R. Graeser. Capturing tumor complexity *in vitro*: comparative analysis of 2D and 3D tumor models for drug discovery, Scientific Reports. 6 (2016): 28951.

86. F. Pampaloni, E. G. Reynaud, E. H. K. Stelzer. The third dimension bridges the gap between cell culture and live tissue, Nature Reviews Molecular Cell Biology. 8, 10 (2007): 839–845.

87. B. M. Baker, C. S. Chen. Deconstructing the third dimension: how 3D culture microenvironments alter cellular cues, Journal of Cell Science. 125, 13 (2012): 3015–3024.

88. J. A. Hickman, R. Graeser, R. Hoogt, S. Vidic, C. Brito, M. Gutekunst, H. Kuip. Three-dimensional models of cancer for pharmacology and cancer cell biology: Capturing tumor complexity *in vitro/ex vivo*, Biotechnology Journal. 9, 9 (2014): 1115–1128.

89. M. J. Bissell, A. Rizki, I. S. Mian. Tissue architecture: the ultimate regulator of breast epithelial function, Current Opinion in Cell Biology. 15, 6 (2003): 753–762.

90. K. Mark, V. Gauss, H. Mark, P. Müller. Relationship between cell shape and type of collagen synthesised as chondrocytes lose their cartilage phenotype in culture, Nature.

267, 5611 (1977): 531–532.

91. M. Kapałczyńska, T. Kolenda, W. Przybyła, M. Zajączkowska, A. Teresiak, V. Filas, M. Ibbs, R. Bliźniak, Ł. Łuczewski, K. Lamperska. 2D and 3D cell cultures—a comparison of different types of cancer cell cultures, Archives of Medical Science: AMS. 14, 4 (2016): 910–919.
92. K. M. A. Yong, Y. Zeng, D. Vindivich, J. M. Phillip, P. Wu, D. Wirtz, R. H. Getzenberg. Morphological effects on expression of growth differentiation factor 15 (GDF15), a marker of metastasis, Journal of Cellular Physiology. 229, 3 (2014): 362–373.
93. R. Edmondson, J. J. Broglie, A. F. Adcock, L. Yang. Three-dimensional cell culture systems and their applications in drug discovery and cell-based biosensors, ASSAY and Drug Development Technologies. 12, 4 (2014): 207–218.
94. K. Chwalek, L. J. Bray, C. Werner. Tissue-engineered 3D tumor angiogenesis models: potential technologies for anti-cancer drug discovery, Advanced Drug Delivery Reviews. 79–80 (2014): 30–39.
95. E. L. S. Fong, D. A. Harrington, M. C. F. Carson, H. Yu. Heralding a new paradigm in 3D tumor modeling, Biomaterials. 108 (2016): 197–213.
96. V. Brancato, J. M. Oliveira, V. M. Correlo, R. L. Reis, S. C. Kundu. Could 3D models of cancer enhance drug screening? Biomaterials. 232 (2019): 119744.
97. M. Simian, Y. Hirai, M. Navre, Z. Werb, A. Lochter, M. J. Bissell. The interplay of matrix metalloproteinases, morphogens and growth factors is necessary for branching of mammary epithelial cells, Development. 128, 16 (2001): 3117–3131.
98. J. E. Fata, H. Mori, A. J. Ewald, H. Zhang, E. Yao, Z. Werb, M. J. Bissell. The MAPK(ERK-1,2) pathway integrates distinct and antagonistic signals from TGFalpha and FGF7 in morphogenesis of mouse mammary epithelium, Developmental Biology.

306, 1 (2007): 193–207.

99. E. Y. Lasfargues. Cultivation and behavior in vitro of the normal mammary epithelium of the adult mouse, The Anatomical Record. 127, 1 (1957): 117–129.

100. S. Ghosh, G. Spagnoli, I. Martin, S. Ploegert, P. Demougin, M. Heberer, A. Reschner. Three-dimensional culture of melanoma cells profoundly affects gene expression profile: a high density oligonucleotide array study, Journal of Cellular Physiology. 204, 2 (2005): 522–531.

101. H. B. Frieboes, X. Zheng, C. Sun, B. Tromberg, R. Gatenby, V. Cristini. An integrated computational/experimental model of tumor invasion, Cancer Research. 66, 3 (2006): 1597–1604.

102. H. Marushima, S. Shibata, T. Asakura, T. Matsuura, H. Maehashi, Y. Ishii, H. Eda, K. Aoki, Y. Iida, T. Morikawa, K. Ohkawa. Three-dimensional culture promotes reconstitution of the tumor-specific hypoxic microenvironment under TGFβ stimulation, International Journal of Oncology. 39, 5 (2011): 1327–1336.

103. X. Huang, Z. Huang, W. Gao, W. Gao, R. He, Y. Li, R. Crawford, Y. Zhou, L. Xiao, Yin Xiao. Current advances in 3D dynamic cell culture systems, Gels. 8, 12 (2022): 829.

104. D. Antoni, H. Burckel, E. Josset, G. Noel. Three-dimensional cell culture: a breakthrough *in vivo*, International Journal of Molecular Sciences. 16 (2015): 5517–5527.

105. S. B. Pasco, S. Brézillon, B. Brassart, L. Ramont, J. B. Oudart, J. C. Monboisse. Tumor microenvironment: extracellular matrix alterations influence tumor progression, Frontiers in Oncology. 10, 397 (2020).

106. R. Baghban, L. Roshangar, R. J. Esfahlan, K. Seidi, A. E. kalan, M. Jaymand, S.

Kolahian, T. Javaheri, P. Zare. Tumor microenvironment complexity and therapeutic implications at a glance, Cell Communication and Signaling: CCS. 18, 1 (2020): 1–19.

107. T. J. Puls, X. Tan, M. Husain, C. F. Whittington, M. L. Fishel, S. L. V. Harbin. Development of a novel 3D tumor-tissue invasion model for high-throughput, high-content phenotypic drug screening, Scientific Reports. 8, 1 (2018): 13039.

108. F. Bray, J. Ferlay, I. Soerjomataram, R. L. Siegel, L. A. Torre, A. Jemal. Global cancer statistics 2018: GLOBOCAN estimates of incidence and mortality worldwide for 36 cancers in 185 countries, CA: A Cancer Journal for Clinicians. 68, 6 (2018): 394–424.

109. S. Rosen, B. K. Brisson, A. C. Durham, C. M. Munroe, C. J. McNeill, D. Stefanovski, K. U. Sørenmo, S. W. Volk. Intratumoral collagen signatures predict clinical outcomes in feline mammary carcinoma, PLOS ONE. 15, 8 (2020): e0236516.

110. F. Adega, A. Borges, R. Chaves. Cat mammary tumors: genetic models for the human counterpart, Veterinary Sciences. 3, 3 (2016): 17.

111. C. Nascimento, F. Ferreira. Tumor microenvironment of human breast cancer, and feline mammary carcinoma as a potential study model, Biochimica et Biophysica Acta (BBA) - Reviews on Cancer. 1876, 1 (2021): 188587.

112. L. Jiang, F. Mousawi, X. Yang, S. Roger. ATP-induced Ca^{2+}-signalling mechanisms in the regulation of mesenchymal stem cell migration, Cellular and Molecular Life Sciences. 74, 20 (2017): 3697–3710.

113. N. Kawai, Y. Hirohashi, Y. Ebihara, T. Saito, A. Murai, T. Saito, T. Shirosaki, T. Kubo, M. Nakatsugawa, T. Kanaseki, T. Tsukahara, T. Shichinohe, L. Li, S. Hirano, T. Torigoe. ABCG2 expression is related to low 5-ALA photodynamic diagnosis (PDD)

efficacy and cancer stem cell phenotype, and suppression of ABCG2 improves the efficacy of PDD, PLOS ONE. 14, 5 (2019): e0216503.

114. T. Osaki, I. Yokoe, Y. Sunden, U. Ota, T. Ichikawa, H. Imazato, T. Ishii, K. Takahashi, M. Ishizuka, T. Tanaka, L. Li, M. Yamashita, Y. Murahata, T. Tsuka, K. Azuma, N. Ito, T. Imagawa, Y. Okamoto. Efficacy of 5-aminolevulinic acid in photodynamic detection and photodynamic therapy in veterinary medicine, Cancers (Basel). 11, 4 (2019): 495.

115. T. Teshigawara, M. Mizuno, T. Ishii, Y. Kitajima, F. Utsumi, J. Sakata, H. Kajiyama, K. Shibata, M. Ishizuka, F. Kikkawa. Novel potential photodynamic therapy strategy using 5-Aminolevulinic acid for ovarian clear-cell carcinoma, Photodiagnosis and Photodynamic Therapy. 21 (2018): 121–127.

116. N. Kramer, A. Walzl, C. Unger, M. Rosner, G. Krupitza, M. Hengstschläger, H. Dolznig. *In vitro* cell migration and invasion assays, Mutation Research/Reviews in Mutation Research. 752, 1 (2013): 10-24.

117. L. G. Griffith, M. A. Swartz. Capturing complex 3D tissue physiology *in vitro*, Nature Reviews Molecular Cell Biology. 7, 3 (2006): 211–224.

118. E. C. Costa, A. F. Moreira, D. M. Diogo, V. M. Gaspar, M. P. Carvalho, I. J. Correia. 3D tumor spheroids: an overview on the tools and techniques used for their analysis, Biotechnology Advances. 34, 8 (2016): 1427–1441.

119. D. V. LaBarbera, B. G. Reid, B. H. Yoo. The multicellular tumor spheroid model for high-throughput cancer drug discovery, Expert Opinion Drug Discovery. 7, 9 (2012): 819–830.

120. C. S. Szot, C. F. Buchanan, J. W. Freeman, M. N. Rylander. 3D in vitro bioengineered tumors based on collagen I hydrogels, Biomaterials. 32, 31 (2011): 7905–7912.

121. K. M. Yamada, E. Cukierman. Modeling tissue morphogenesis and cancer in 3D, Cell. 130, 4 (2007): 601–610.

122. F. Xu, K. J. L. Burg. Three-dimensional polymeric systems for cancer cell studies, Cytotechnology. 54, 3 (2007): 135–143.

123. R. W. K. Wu, E. S. M. Chu, J. W. M. Yuen, Z. Huang. Comparative study of FosPeg® photodynamic effect on nasopharyngeal carcinoma cells in 2D and 3D models, Journal of Photochemistry and Photobiology B: Biology. 210 (2020): 111987.

124. Y. Imamura, T. Mukohara, Y. Shimono, Y. Funakoshi, N. Chayahara, M. Toyoda, N. Kiyota, S. Takao, S. Kono, T. Nakatsura, H. Minami. Comparison of 2D- and 3D-culture models as drug-testing platforms in breast cancer, Oncology Reports. 33, 4 (2015): 1837–1843.

125. R. K. Jain. Normalization of tumor vasculature: an emerging concept in antiangiogenic therapy, Science. 307, 5706 (2005): 58–62.

126. L. Rodriguez, A. Batlle, G. D. Venosa, A. J. MacRobert, S. Battah, H. Daniel, A. Casas. Study of the mechanisms of uptake of 5-aminolevulinic acid derivatives by PEPT1 and PEPT2 transporters as a tool to improve photodynamic therapy of tumours, The International Journal of Biochemistry & Cell Biology. 38, 9 (2006): 1530–1539.

127. K. Omoto, R. Matsuda, Y. Nakai, Y. Tatsumi, T. Nakazawa, Y. Tanaka, Y. Shida, T. Murakami, F. Nishimura, I. Nakagawa, Y. Motoyama, M. Nakamura, K. Fujimoto, N. Hiroyuki. Expression of peptide transporter 1 has a positive correlation in protoporphyrin IX accumulation induced by 5-aminolevulinic acid with photodynamic detection of non-small cell lung cancer and metastatic brain tumor specimens originating from non-small cell lung cancer, Photodiagnosis and

Photodynamic Therapy. 25 (2019): 309–316.

128. Y. Hagiya, H. Fukuhara, K. Matsumoto, Y. Endo, M. Nakajima, T. Tanaka, I. Okura, A. Kurabayashi, M. Furihata, K. Inoue, T. Shuin, S. Ogura. Expression levels of PEPT1 and ABCG2 play key roles in 5-aminolevulinic acid (ALA)-induced tumor-specific protoporphyrin IX (PpIX) accumulation in bladder cancer, Photodiagnosis and Photodynamic Therapy. 10, 3 (2013): 288–295.

129. C. Hou, S. Yamaguchi, Y. Ishi, S. Terasaka, H. Kobayashi, H. Motegi, K. C. Hatanaka, K. Houkin. Identification of PEPT2 as an important candidate molecule in 5-ALA-mediated fluorescence-guided surgery in WHO grade II/III gliomas, Journal of Neuro-Oncology. 143, 2 (2019): 197–206.

130. H. Kobuchi, K. Moriya, T. Ogino, H. Fujita, K. Inoue, T. Shuin, T. Yasuda, K. Utsumi, T. Utsumi. Mitochondrial localization of ABC transporter ABCG2 and its function in 5-aminolevulinic acid-mediated protoporphyrin IX accumulation, PLOS One. 7, 11 (2012): e50082.

131. Y. Hagiya, Y. Endo, Y. Yonemura, K. Takahashi, M. Ishizuka, F. Abe, T. Tanaka, I. Okura, M. Nakajima, T. Ishikawa, S. Ogura. Pivotal roles of peptide transporter PEPT1 and ATP-binding cassette (ABC) transporter ABCG2 in 5-aminolevulinic acid (ALA)-based photocytotoxicity of gastric cancer cells *in vitro*, Photodiagnosis and Photodynamic Therapy, 9, 3 (2012): 204–214.

132. M. Mazurek, D. Szczepanek, A. Orzyłowska, R. Rola. Analysis of factors affecting 5-ALA fluorescence intensity in visualizing glial tumor cells-literature review, International Journal of Molecular Sciences. 23, 2 (2022): 926.

133. M. Mastrangelopoulou, M. Grigalavicius, T. H. Raabe, E. Skarpen, P. Juzenas, Q. Peng, K. Berg, T. A. Theodossiou. Predictive biomarkers for 5-ALA-PDT can lead

to personalized treatments and overcome tumor-specific resistances, Cancer Reports (Hoboken). 5, 12 (2022): e1278.

134. K. Inoue, H. Fukuhara, S. Yamamoto, T. Karashima, A. Kurabayashi, M. Furihata, K. Hanazaki, H. Lai, S. Ogura. Current status of photodynamic technology for urothelial cancer, Cancer Science. 113, 2 (2022): 392–398.

135. W. H. Koppenol, P. L. Bounds, C. V. Dang. Otto Warburg's contributions to current concepts of cancer metabolism, Nature Reviews Cancer. 11 (2011): 325–337.

136. Y. Ohgari, Y. Miyata, T. Miyagi, S. Gotoh, T. Ohta, T. Kataoka, K. Furuyama, S. Taketani. Roles of porphyrin and iron metabolisms in the δ-aminolevulinic acid (ALA)-induced accumulation of protoporphyrin and photodamage of tumor cells, Photochemistry and Photobiology. 87, 5 (2011): 1138–1145.

137. J. Frank, M. R. L. Schäfer, H. Schöffl, A. Flaccus, C. Lambert, H. K. Biesalski. Inhibition of heme oxygenase-1 increases responsiveness of melanoma cells to ALA-based photodynamic therapy, International Journal of Oncology. 31, 6 (2007): 1539–1545.

138. D. Nowis, M. Legat, T. Grzela, J. Niderla, E. Wilczek, G. M. Wilczynski, E. Głodkowska, P. Mrówka, T. Issat, J. Dulak, A. Józkowicz, H. Waś, M. Adamek, A. Wrzosek, S. Nazarewski, M. Makowski, T. Stokłosa, M. Jakóbisiak, J. Gołab. Heme oxygenase-1 protects tumor cells against photodynamic therapy-mediated cytotoxicity, Oncogene. 25, 24 (2006): 3365–3374.

139. G. A. Hunter, G. C. Ferreira. Pre-steady-state reaction of 5-aminolevulinate synthase. Evidence for a rate-determining product release, The Journal of Biological Chemistry. 274, 18 (1999): 12222–12228.

140. Y. Kubota, K. Nomura, Y. Katoh, R. Yamashita, K. Kaneko, K. Furuyama. Novel

mechanisms for heme-dependent degradation of ALAS1 protein as a component of negative feedback regulation of heme biosynthesis, The Journal of Biological Chemistry. 291, 39 (2016): 20516–20529.

141. G. G. Eskiler, A. D. Ozkan, E. S. Kucukkara, A. F. Kamanlı, B. Gunoğlu, M. Z. Yıldız. Optimization of 5-aminolevulinic acid-based photodynamic therapy protocol for breast cancer cells, Photodiagnosis and Photodynamic Therapy. 31 (2020): 101854.

142. G. G. Eskiler, O. Turna, A. D. Ozkan, A. Baykal, H. O. Gurgen, B. Erk, E. I. Armutak, H. S. Lim. The response of the canine mammary simple carcinoma and carcinosarcoma cells to 5-aminolaevulinic acid-based photodynamic therapy: An *in vitro* study, Journal of Photochemistry and Photobiology. B, Biology. 234 (2022): 112509.

143. H. Mohammadpour, R. Fekrazad. Antitumor effect of combined Dkk-3 and 5-ALA mediated photodynamic therapy in breast cancer cell's colony, Photodiagnosis and Photodynamic Therapy. 14 (2016): 200–203.

Acknowledgments

First, I would like to express my deepest gratitude to my supervisor, Associate Prof. Dr. Tomohiro Osaki, for his guidance and assistance in designing the experiments and using the research equipment. I want to thank my associate supervising professor, Prof. Dr. Takashi Mori and Associate Prof. Dr. Kazuki Harada, for providing advice—sincere thanks to all the lecturing professors during my doctoral program. I want to thank my parents, family, and husband for their support and encouragement.

I am very thankful to the Tottori Univ. Mirai Fund and Rotary Yoneyama Scholar for providing scholarships for one year each during my doctoral course.